Title
Directly Modulated Magnetic Pendulum Arrays for Efficient Ultra Low Frequency Transmission

Author
Mysore Nagaraja, Srinivas Prasad

Publication Date
2020

Peer reviewed|Thesis/dissertation

UNIVERSITY OF CALIFORNIA

Los Angeles

Directly Modulated Magnetic Pendulum Arrays for Efficient Ultra Low Frequency Transmission

A dissertation submitted in partial satisfaction of the

requirements for the degree Doctor of Philosophy

in Electrical and Computer Engineering

by

Srinivas Prasad Mysore Nagaraja

2020

ABSTRACT OF THE DISSERTATION

Directly Modulated Magnetic Pendulum Arrays for Efficient Ultra Low Frequency Transmission

by

Srinivas Prasad Mysore Nagaraja

Doctor of Philosophy in Electrical and Computer Engineering

University of California, Los Angeles, 2020

Professor Yuanxun Wang, Chair

The frequencies lying between 300 Hz to 3 kHz have been designated as Ultra Low Frequency (ULF) with corresponding wavelengths from 1000 Km to 100 Km. Although ULF has very low bandwidth it is very reliable, penetrating and difficult to jam which makes it a great choice for communication in underwater and underground environments. Small and portable ULF antennas within a diameter of 1 meter would operate under an electrical length on the order of 10^{-4} to 10^{-6} wavelengths in free space, making them very inefficient because of fundamental limits on radiation from electrically small antennas. To overcome this problem, Mechanical Antennas or 'Mechtennas' for Ultra Low Frequency Communications have been proposed recently. For efficient generation of ULF radiation, we propose a portable electromechanical system called Magnetic Pendulum Array (MPA) with Direct Antenna Modulation (DAM). MPAs use an array of mechanically oscillating permanent magnets to efficiently generate ULF radiation. Proof of concept demonstrations of the 1D array system and 2D array system at 1kHz

and 700 Hz respectively are presented. A Direct Antenna Modulation (DAM) scheme with Binary Frequency Shift Keying is implemented achieving a data rate of 18 bps on the 2D array system. The theory and experimental results demonstrate that such a system can achieve a significantly higher quality factor than conventional coils and thus order of magnitude higher transmission efficiency. The concept can be easily scaled to the ULF range of frequencies with more complicated modulation schemes for higher data rates.

The dissertation of Srinivas Prasad Mysore Nagaraja is approved.

Yahya Rahmat Samii

Christopher S. Lynch

Subramanian Srikantes Iyer

Yuanxun Wang, Committee Chair

University of California, Los Angeles

2020

This dissertation is dedicated to my parents,

who are a constant source of support and encouragement.

TABLE OF CONTENTS

LIST OF FIGURES

LIST OF TABLES

SYMBOLS AND ACRONYMS

1-D/2-D	One-/Two-Dimensional
AWG	American Wire Gauge
DAM	Direct Antenna Modulation
DC	Direct Current
ELF	Extremely Low Frequency
EM	Electromagnetic
MW	Mega Watt
NdFeB	Neodymium Iron Boron
Q factor	Quality Factor
RF	Radio Frequency
ULF	Ultra-Low Frequency
VLF	Very Low Frequency

ACKNOWLEDGEMENTS

First and foremost, I express my heartfelt gratitude to my advisor Prof. Yuanxun 'Ethan' Wang for his relentless efforts in guiding me through these years. His excitement, dedication and passion for research continues to inspire me. I also would like to acknowledge Prof. Yahya Rahmat Samii, Prof. Christopher Lynch and Prof. Subramanian Iyer for serving as my doctoral committee members and giving me insightful comments and advice.

I am grateful to my outstanding collaborators for their indispensable support and contribution to my research work. I would like to thank Scott Bland and Adam Propst at Nextgen Aeronautics for their fabrication and characterization support.

None of my work would have been possible without the support of my lab mates, who have become my family here at UCLA. The work presented here is a byproduct of countless fruitful discussions I have had with my lab mates. I especially thank Dr. Rustu Umut Tok and Dr. Foad Fereidoony for their continuous guidance and support throughout my time in the lab. I would also like to thank Minji Zhu, the lab manager of the Center for High Frequency Electronics (CHFE) at UCLA, for his support with the measurement equipment. I also gratefully acknowledge financial support for this work by the DARPA AMEBA program (Grant No: HR0011-17-C-0108)

I am grateful to my parents for their eternal love, support and encouragement. Lastly, I would like to thank all my friends and administrative staff at UCLA, who formed the support system needed for my work.

VITA

Education

2017-2020	***PhD candidate*** in **Electrical and Computer Engineering**
	University of California, Los Angeles, USA
2015-2017	***M.S.*** in **Electrical Engineering**
	University of California, Los Angeles, USA
2011-2015	***B.E. (Hons)*** in **Electrical and Electronics Engineering**
	Birla Institute of Technology and Science, Pilani, India.

Selected Publications

[1] **Srinivas Prasad M N**, Rustu Umut Tok, Foad Fereidoony, Yuanxun Ethan Wang, Rui Zhu, Adam Propst and Scott Bland, "Magnetic Pendulum Arrays for Efficient ULF Transmission", Sci. Rep., vol. 9, p.13220, Sep. 2019.

Conference Presentations

[1] **Srinivas Prasad M N**, Rustu Umut Tok, Rui Zhu, Scott Bland, Adam Propst and Y. E. Wang, "Magnetic Pendulum Arrays for Efficient Wireless Power Transmission," 2018 PowerMEMS, Daytona Beach, USA, Dec 4–Dec 7, 2018.

[2] **Srinivas Prasad M N**, Rustu Umut Tok and Y. E. Wang, "Magnetic Pendulum Arrays for ULF Transmission," 2018 IEEE International Symposium on Antennas and Propagation & USNC/URSI National Radio Science Meeting, Boston, USA, July 8–July 13, 2018.

[3] **Srinivas Prasad M N,** Skyler Selvin, Rustu Umut Tok, Yikun Huang and Y. E. Wang, "Directly Modulated Spinning Magnet Arrays for ULF Communications," 2018 IEEE Radio and Wireless Symposium (RWS), Anaheim, USA, January 17th, 2018.

[4] **Srinivas Prasad M N,** Yikun Huang and Y. E. Wang, "Going Beyond Chu Harrington Limit: ULF Radiation with a Spinning Magnet Array," 2017 XXXIInd General Assembly and Scientific Symposium of the International Union of Radio Science (URSI GASS), Montreal, Canada, Aug 19–Aug 26, 2017.

Chapter 1

Introduction

1.1 Why ULF?

It becomes impractical to use conventional Radio Frequency (RF) transmission and reception in underwater and underground communications as the medium can distort and, in many cases, completely block the signals from propagating between the transmitter and receiver in such environments. The very same physics which makes RF communication possible also imposes some strict limits on propagation of electromagnetic waves when they encounter materials like water, soil or stone which block or attenuate the radio signals. The skin depth (δ) equation given by $\delta = \frac{1}{\sqrt{\pi f \mu \sigma}}$ where f is the frequency of the field, μ is the magnetic permeability of the material and σ is the conductivity of the material [1] clearly demonstrates the large attenuation of the high frequency electromagnetic fields. For example, the skin depth for a 100 MHz signal is about three orders of magnitude smaller as compared to the skin depth of a 1 kHz signal in the same medium. The large attenuation of electromagnetic waves in ocean water is due to its high conductivity. Fig 1.1 is a composite sketch of the attenuation of a plane electromagnetic wave in sea water as a function of frequency. We can clearly see from the figure that only at Ultra Low frequencies and at optical frequencies is the attenuation low enough to allow useful penetration. Other natural media such as soil and rock typically have much smaller conductivities as can be seen in Table 1.1 [3]. Thus, it is advantageous to use low frequency signals when the medium has strong absorption. Frequencies lying between 300 Hz to 3 kHz have been designated as Ultra Low Frequency (ULF), with corresponding wavelengths from

1000 Km to 100 Km. Radio signals at these frequencies can penetrate some distance into media such as water, soil, and rock.

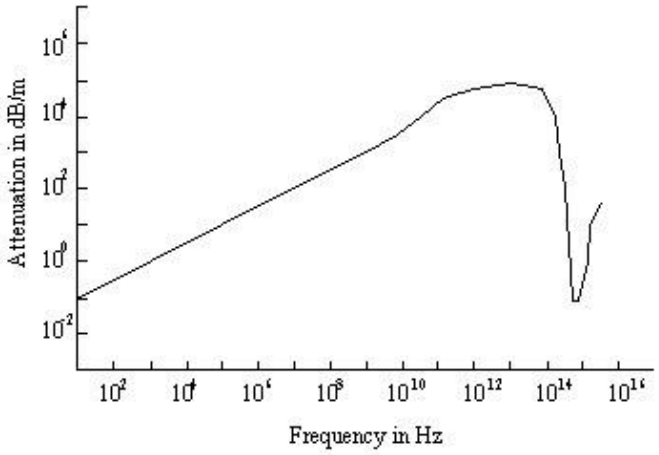

Figure 1.1: Attenuation of EM wave passing through Sea Water (adapted from [2])

Although ULF has limited bandwidth, and thus low data rates, it is an attractive choice for underwater and underground environments where high frequency radio signals cannot reach as ULF is reliable, can penetrate these media, and difficult to interfere with. ULF is advantageous over the use of acoustic waves because it is immune from the reverberation associated with acoustic waves, especially in and around the obstacles such as bridges and vessel hulls. Therefore, ULF has been widely used for military applications involving long range communications with submarines and underground mines.

1.1.1 ULF Communication Antennas: Current state of the art

For considering ULF communication links with practical applications rather than pure academic interest existence of practical transmitting and receiving antennas is required. To date

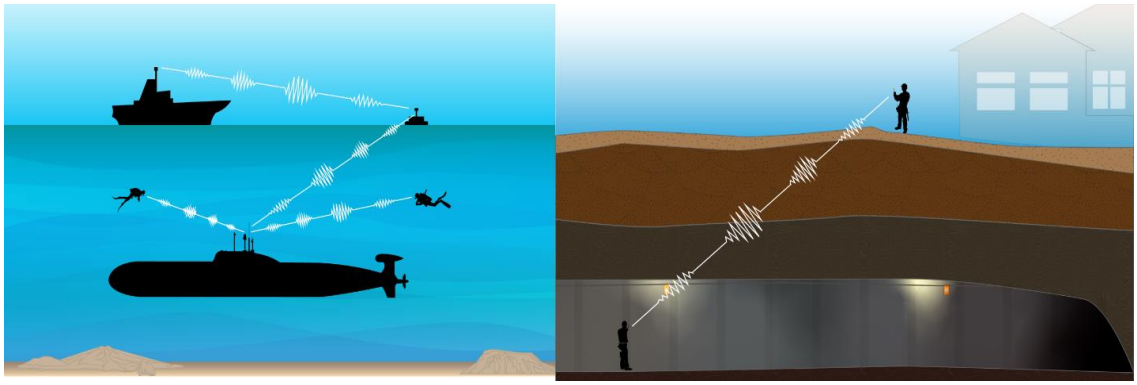

Figure 1.2: ULF antennas can enable underwater and underground communications.

Table 1.1: Conductivities of Earth Media

Medium	**Conductivities (S/m)**	
	Typical	**Extremes**
Rock	10^{-1} to 10^{-3}	> 1 to $< 10^{-4}$
Soils	10^{-2} to 10^{-3}	$> 10^{-1}$ to $< 10^{-3}$
Sea Water	4	3 to 5

construction of ULF transmitters is extremely costly as the wavelength at these frequencies rival distances between cities and states. It is well known that the size of the antenna is proportional to the wavelength at which it operates, so communications at ULF has resulted in the construction of gigantic antennas which consume Megawatts of power. An efficient ULF antenna would be prohibitively large making it impractical to build. Any practical electrically small antenna would

be very inefficient because the radiated power is now a tiny fraction of the stored energy on the antenna according to Chu's limit [4] while the dissipated power is usually a much greater fraction of the same energy given by the finite quality (Q) factor of the material that comprises the antenna. The former ratio can be increased by reducing the radiation quality factor, i.e., increasing the electrical dimension of the antenna. Portable receivers at ULF which use magnetic sensors are available. This thesis addresses the challenge of building portable, low cost and low power ULF transmitters.

The U.S. Navy's Very Low Frequency (VLF, 3 – 30 kHz) antenna in Cutler, Maine shown in Fig. 1.3 occupies 2000 acres on a peninsula and consists of 26 towers, each 850 to 1000ft high. It consumes 18 MW power from a dedicated power plant [5]. On the other hand, the radiation efficiency can also be enhanced with the use of a higher quality factor transmitting antenna [6].

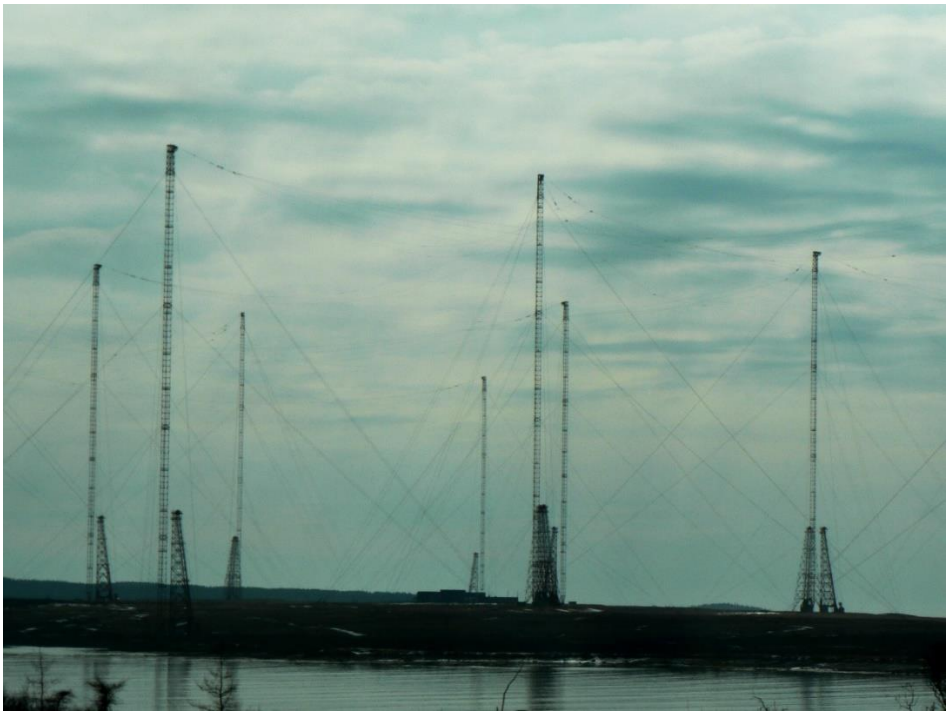

Figure 1.3: US Navy's VLF antenna in Cutler, Maine.

A space borne antenna for ULF/VLF radiation has been described in [7]. It consists of a superconducting DC rotating coil surrounded by magneto plasma operating as an ULF transmitter. It has been shown that such a space-borne antenna is not engineeringly feasible [7]. A novel phased orthogonal loop antenna is used to create a rotating magnetic field source, which creates low frequency waves called Alfven waves (80 to 355 kHz) as described in [8]. It requires a high power LRC driver circuit with peak-to-peak current of 1200 A and voltages across the capacitors of 2000 V. Reference [9] describes magnetic antennas for ULF and VLF radiation which uses multiple loops wound around a magnetic core which can be used for through the earth communications.

1.2 Introduction to Mechanical Antennas

The classical idea behind antenna radiation has been time varying currents. Conventional antennas such as dipoles and loops generate propagating electromagnetic waves from conductive currents exposed in free space. A novel method of using the mechanical motion of charges to produce ULF radiation has recently gained momentum. The difference between a conventional electrically small antenna and a ‘mechtenna’ lies in the fact that conventional antennas create dynamic electromagnetic fields by relying on field-accelerated charges, whereas in mechtennas radiated time-varying fields are generated by physically moving, rotating or oscillating the electric charges or magnetic dipole moments as shown in Fig 1.4.

The radiation efficiency of a conventional electrically small antenna is limited by its ohmic loss, which is the dominating loss mechanism. It will be shown that such ohmic loss can be overcome by mechanical antennas. The key for high efficiency mechanical antennas lies in the development of a high-quality factor (high - Q) mechanical oscillatory system that has extremely

small damping and effectively couples to the changing dipole moments. Several mechanical antennas, or ‘mechtennas’, have been proposed. Spinning magnet antennas have been used for generation of Extremely Low Frequency (ELF) and ULF radiation in [10-17]. These systems use either a single rotating magnet or an array of rotating magnets to produce low frequency fields. Fig 1.5 shows an example of a Spinning Magnet Antenna and a Spinning Magnet Array used in [13]. Electrets are highly resistive dielectric materials which quasi-permanently immobilize charge within their structure [18]. Use of linearly actuated and rotating electrets for ULF radiation has been described in [18]. Use of piezo electric and magneto electric materials driven at acoustic resonance for VLF transmission has been described in [19-20]. Most of the proposed mechtennas utilize either rotating electric or magnetic dipoles or piezo electric materials driven at acoustic resonance for generating low frequency radiation.

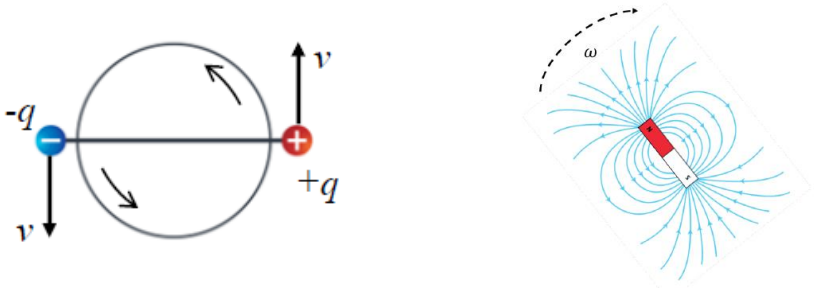

(a) Spinning Electric dipole (b) Spinning magnet

Figure 1.4: Spinning magnetic or electric dipoles can create low frequency radiation.

The rotating systems require a great amount of mechanical energy to be injected before the antenna rotates at the desired speed. They are inefficient when modulation is introduced. The charge stability in electret based mechtennas is of concern as electrets lose their charge over a period based on the type of material and many environmental factors such as temperature,

moisture and humidity. The piezo electric systems have been demonstrated at Very Low Frequency (3 kHz to 30 kHz) range but they have the potential of working at ULF range. This work focuses on an innovative mechanically driven transmitter not consisting of rotating magnets or piezo electric materials but rather consists of an array of magnetic pendulums in oscillatory motion at ULF. There are several merits when a pendulum-based system over a rotating magnet based mechtenna is used. The first merit is that in a pendulum the stored energy and the mechanical motion in such a system is built up gradually at a constant frequency. The pendulums can form an array easily without the need for maintaining axially symmetry. Consequently, the total effective magnetic dipole moment remains the same while stored energy per unit volume reduces as the dimension of each pendulum reduces [21]. The third advantage is that the stored energy in a pendulum system alternates between two states, namely the kinetic energy due to inertia and the magnetic potential energy due to the magnetic field re-distribution. This allows one to control the motion and to enforce modulation to the radiation through the so-called Direct Antenna Modulation (DAM) approach [22]. Finally, the pendulums require no electric motor to drive and the only dominant loss mechanism in the proposed magnetic pendulum array is the friction of the pendulum supporting bearings. Hence, one can achieve a very high-Q factor in such a system that will greatly enhance the transmission efficiency for near-field ULF communications.

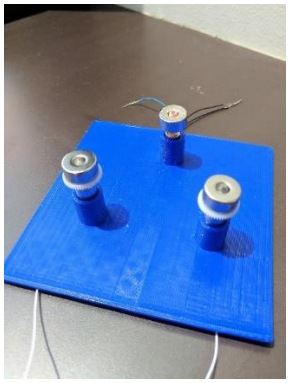

(a) Spinning Magnet Antenna (b) Spinning Magnet Array

Figure 1.5: Spinning Magnet Antennas mounted on motors.

1.3 Dissertation Outline

This thesis focuses on an innovative mechanically driven transmitter not consisting of rotating magnets or piezo electric materials but rather consists of an array of magnetic pendulums in oscillatory motion with Direct Antenna Modulation (DAM) for near field ULF communications. In Chapter 2, we will first present the details of the proposed system design using magnetic pendulum arrays. We also present the analytical calculation of the resonant frequency of the 1D magnetic pendulum arrays. The chapter also details the swing angle calculation and the relation between Q factor and the various system parameters. Modeling of magnetic pendulum arrays is an important aspect of system design. In Chapter 3 the modelling and simulation of magnetic pendulum arrays using full wave simulation tools is presented. Ansys Maxwell 2D is used to simulate 1D magnetic pendulum arrays. Based on the simulation results a 28-element pendulum array is fabricated. In Chapter 4, the measured results of 1D magnetic pendulum arrays are presented based on the 28-element prototype along with a circuit model. The equivalent circuit model of the system will aid in understanding the system in an intuitive

way and would be a great tool to quickly verify some of the properties of the system. 1D pendulum arrays were scaled up to achieve higher transmitted fields by extending the array in two dimensions. A prototype of 5X11 array consisting of 55 elements is fabricated and measured. In Chapter 5 we present the design, modelling and measured results of 2D magnetic pendulum arrays along with its circuit model. BFSK modulation was implemented with the DAM scheme on the 5X11 array prototype achieving a data rate of 18 bps. DAM implementation and measured results of the modulated signal are presented in Chapter 6. Finally, a brief discussion and conclusion will be given in Chapter 7, along with a summary and outlook of future research work.

Chapter 2

Proposed System Design with Magnetic Pendulum Arrays

Mechanical antennas, as mentioned earlier, rely on physically moving electric charges or magnetic dipole moments through oscillatory mechanical movements to generate a dynamic electromagnetic field, which avoids the ohmic loss of a conventional conductor-based antenna. Mechanical antennas based on rotating magnets have been proposed in [10-17]. A spinning magnetic dipole field can be represented by superposition of two orthogonal magnetic dipole solutions in space with a 90-degree phase [11]. Assuming, the rotation is with an angular frequency ω, the following electromagnetic fields can be obtained for an oscillating magnetic dipole at a distance r:

$$\vec{E} = \frac{\mu_o m_o sin\theta}{4\pi r}\left[\frac{\omega^2}{c}\cos\left(\omega\left(t-\frac{r}{c}\right)\right)+\frac{\omega}{r}\sin\left(\omega\left(t-\frac{r}{c}\right)\right)\right]\hat{\phi} \quad (1)$$

$$\vec{B} = \frac{\mu_o m_o cos\theta}{2\pi r^2}\left[\frac{1}{r}\cos\left(\omega\left(t-\frac{r}{c}\right)\right)-\frac{\omega}{c}\sin\left(\omega\left(t-\frac{r}{c}\right)\right)\right]\hat{r}+$$

$$\frac{\mu_o m_o sin\theta}{4\pi r}\left[\left(\frac{1}{r^2}-\frac{\omega^2}{c^2}\right)\cos\left(\omega\left(t-\frac{r}{c}\right)\right)-\frac{\omega}{rc}\sin\left(\omega\left(t-\frac{r}{c}\right)\right)\right]\hat{\theta} \quad (2)$$

In the far field we can obtain the following expressions for the radiated fields $\vec{E}_{rad}$ and $\vec{B}_{rad}$ for a rotating magnetic dipole assuming the observer is much further away than the wavelength ($r \gg c/\omega$)

$$\vec{B}_{rad} = \frac{\mu_o m_o \omega^2}{4\pi r c^2}\left[\cos\left(\omega\left(t-\frac{r}{c}\right)\right)\left(\hat{x}-\frac{x}{r}\hat{r}\right)+\sin\left(\omega\left(t-\frac{r}{c}\right)\right)\left(\hat{y}-\frac{y}{r}\hat{r}\right)\right] \quad (3)$$

$$\vec{E}_{rad} = -c\left(\hat{r}\times\vec{B}_{rad}\right) \quad (4)$$

where μ_o is the permeability of free space, m_o is the magnetic dipole moment and c is the speed of light in vacuum. Therefore, the spinning magnet will generate a circularly polarized electromagnetic wave in the far field at the direction normal to the rotation plane or linear polarization in the plane of rotation that can be used for far-field communications. In the near field, the magnetic field component dominates, and one may obtain the near field by rotating the magnetic dipole field expression according to the rotational axis, yielding

$$\vec{B} = \frac{\mu_o m_o cos\theta}{2\pi r^3}\left[\cos\left(\omega\left(t-\frac{r}{c}\right)\right)\right]\hat{r}+\frac{\mu_o m_o sin\theta}{4\pi r^3}\left[\cos\left(\omega\left(t-\frac{r}{c}\right)\right)\right]\hat{\theta} \quad (5)$$

It is evident that in the near field the longitudinal B field component can be best used for ULF communications. The unique characteristic of spinning magnet as shown in Fig 2.1(a) is that the magnetic near field has the stored electromagnetic energy which does not require pairing with another form of energy and is constant irrespective of the angular frequency of rotation and orientation. We can ignore the mechanical energy required for spinning the magnet if the magnetization to mass ratio is high enough. But spinning magnet systems have many disadvantages associated with them. In practice, to transmit an ULF signal at 1 kHz we would have to rotate the magnets at the speed of 60,000 rpm, which is not trivial from a mechanical design perspective. The system must be designed in a such way that the frictional energy losses are minimized, and the tensile stress limits are met. An even more fundamental issue associated with the spinning magnet system is that the dynamic magnetic energy created can get overwhelmed by the mechanical energy required to spin the magnet to designated speed [14].

Introduction of modulation of angular velocity would require replenishment of the energy difference which might get dissipated between the two modulation states leading to lower efficiency of the system. The total mechanical energy W_{ME} associated with a circular disc of radius r, mass m and volume V, rotating at an angular velocity ω can be written as

$$W_{ME} = \frac{1}{2} I\omega^2 \qquad (6)$$

where $I = \frac{mr^2}{2}$ is the moment of inertia of the magnets.

We can write the average energy density as

$$\frac{W_{ME}}{V} = \frac{1}{4}\omega^2 r^2 \rho \qquad (7)$$

For a circular Neodymium based magnet with a radius of 0.5 m, height 1 cm and mass density 7500 kg/m^3 spinning at 1 kHz, the approximate mechanical energy density on an average is $1.85 \times 10^7\ KJ/m^3$ and the total mechanical energy is $1.45 \times 10^8\ J$. In comparison, the typical energy density of an NdFeB magnet obtained from its BH_{max} value is around 470 kJ/m^3 [23]. The five orders of magnitude energy density difference in a spinning magnet implies that most of the energy in the system remains in the mechanical domain rather than the magnetic domain, thus is inefficient in creating electromagnetic coupling or radiation. One could make a case for a spinning magnet array consisting of an array of synchronously rotating smaller magnets which can not only emulate a larger spinning disc with the same volume and having the same magnetic field behavior but also lower the mechanical energy density significantly, as shown in Fig.2.1(b). For example, consider an array of spinning magnets each having a radius of 5 mm and height 1cm. A quick calculation indicates that we need 10,000 such magnets to have the same volume

as compared to a spinning magnet previously described. At 1 kHz, the total mechanical energy is $1.45 \times 10^4 J$ which is much lower than the spinning magnet of 0.5 m radius but the mechanical energy density of each magnet is $1.85 \times 10^5\ KJ/m^3$ which is still higher than the magnetic energy density. At 100 Hz, the mechanical energy density per magnet is $18\ kJ/m^3$ and is one order of magnitude lower than the magnetic energy density. Thus, it is possible to pursue spinning magnet arrays at lower frequencies (100 Hz) but not at higher ULF (1 kHz). Also, in this case the original axial symmetry of the system is broken which would create energy peaks and wells at different angles that prohibit an energy free rotation. The efficiency of a motor driving these magnets will also be problematic as it is at free running conditions. Any further reduction in size of the motor driven spinning magnet will also be impractical from the manufacturing perspective due to the prohibitive complexity. Modulating spinning magnets is difficult since all the parts are in a constant, high angular velocity motion.

To realize an ULF mechtenna with high radiation efficiency, a high-Q mechanical system that is easy to control is necessary. Pendulums are well-known to be high-Q and likewise a magnetic pendulum consisting of a diametrically magnetized cylinder and a pair of external magnets shown in Fig.2.1 (c) is one of such high-Q systems. The external magnets would align the cylinder to a direction of south to north and north to south and any disturbance to that equilibrium condition with external excitation will create an oscillatory swinging motion of the cylindrical magnet. The idea can be further extended to an array of such magnetic pendulums in smaller diameters which not only reduces the total mechanical energy and mechanical energy density of the system as shown earlier but also eliminates the need for external biasing magnets. As shown in Fig 2.1 (d), the system consists of cylindrical magnets which are diametrically magnetized and arranged in an array fashion. The array is said to be self-biased as a static

external magnetic field is not required for their alignment. The alignment of each magnet in the array to the array axis occurs by itself due to the field of the adjacent magnets. An external coil is placed around the housing in the plane of the magnets to excite the magnets to create a time-varying magnetic field B_{RF} that is perpendicular to the pendulum array plane, which can physically rotate the magnets' magnetic orientation towards the out of plane direction.

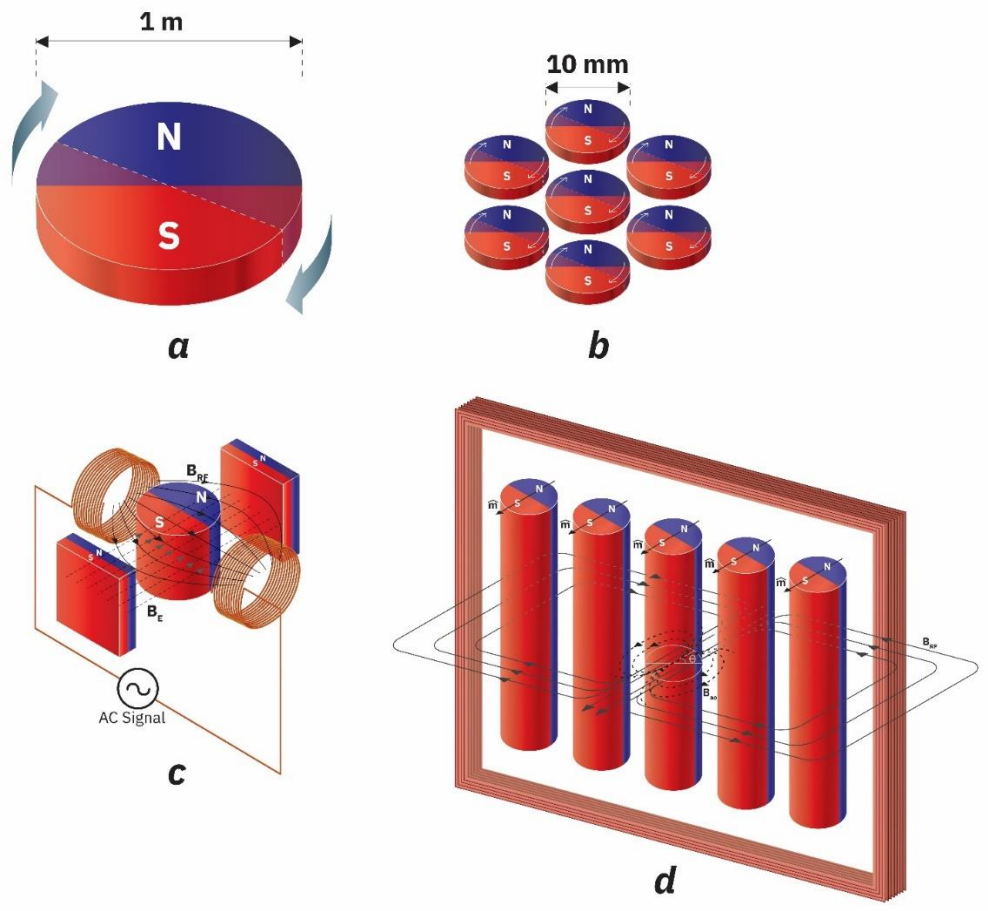

Figure 2.1: Evolution of Self Biased Magnetic Pendulum Array. (a) Spinning magnet driven by external motor. (b) An array of spinning magnets driven by external motors. (c) Externally biased magnetic pendulum driven by an external AC field. (d) Self-biased magnetic pendulum array driven by and external AC field.

In general, the magnitude of the radio frequency magnetic field is much lower than the magnitude of DC magnetic field, but in a high Q system the RF magnetic field can substantially deviate the magnets away from their lowest energy state eventually, as oscillatory motion is built up given enough excitation time [21]. The RF coil injects the RF energy that is not only needed to build up the oscillatory motion but also to replenish any losses in the form of friction loss or eddy current loss, including the RF energy that is radiated and dissipated after the magnetic pendulum array reaches its steady state [21]. The frictional and eddy current losses can be minimized to be an extremely small fraction of energy in the system with proper design. A dynamic magnetic field is created in the out of plane direction due to the oscillatory motion of the magnets [21] which can be used for near field communication and energy transfer. We hypothesize that such a self-biased magnetic pendulum array can create 100% mechanical-to-magnetic coupling and a high Q vibration of the magnetic field for efficient ULF transmission. Note that the magnets can be arranged along just one dimension resulting in 1D Magnetic Pendulum Arrays or can be stacked along two dimensions resulting in 2D stacked pendulum arrays. In the following section we calculate the resonant frequency of the Magnetic Pendulum Array.

2.1 Resonant frequency calculation of Magnetic Pendulum Arrays

The resonant frequency of the Magnetic Pendulum Arrays can be derived based on the interaction of the magnets with each other. Second order differential equations are solved based on the torque between the magnets to obtain the frequency of oscillation for the 1D Magnetic Pendulum Arrays. The resonant frequency calculation for the 2D arrays is presented in a later chapter.

2.1.1 1-D MPA resonant frequency calculation

The angular acceleration of a mass is governed by

$$\frac{d^2\theta}{dt^2} I = -T \qquad (8)$$

where I is the angular moment of inertia and T is a torque on the rotating mass. A pendulum with cylindrical shape has a moment of inertia

$$\mathrm{I} = \frac{m_a r^2}{2} \qquad (9)$$

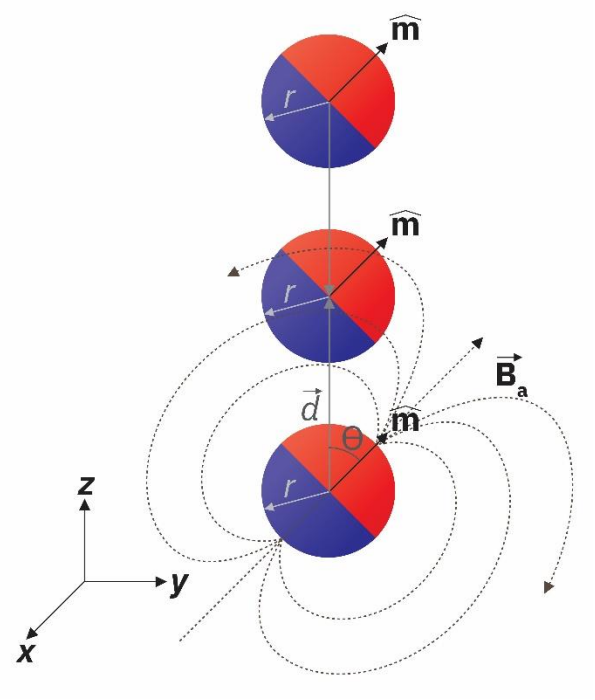

Figure 2.2: Magnetic field experienced by each magnet due to the adjacent magnet.

where m_a is the mass and r is the radius of the cylinder. This differential equation results in a second order system with oscillatory solutions when the torque is a function of angular position. The magnetic pendulum receives a magnetic torque $\vec{T}$ given by

$$\vec{T} = \vec{m} \times \vec{B} \qquad (10)$$

where $\vec{m}$ is the magnetic dipole moment and $\vec{B}$ is the magnetic field, which can be an external field added through a biasing magnet or an internal field created by the neighboring pendulums.

For a single pendulum in a uniform external magnetic field B_e, the pendulum equation can be shown as:

$$\frac{d^2\theta}{dt^2} = -\frac{2M_sB_e}{\rho r^2}\theta \qquad (11)$$

where M_s is the saturation magnetization and ρ is the mass density. The solution to the swing angle θ is given by

$$\theta(t) = \theta_{\max} \sin\left(\frac{1}{r}\sqrt{\frac{2M_sB_e}{\rho}}t\right) \qquad (12)$$

For the magnetic pendulum array as shown in Fig 2.2, the magnetic field from adjacent magnets can play a significant role as it is interacting with the pendulum's motion. Considering the magnetic field generated at each pendulum by an adjacent pendulum that is placed along the longitudinal axis (θ = 0) at distance d as shown in Fig 2.2, The magnetic field experienced by each magnet due to its adjacent magnets can be written in the form of a magnetic dipole field as:

$$\vec{B}_a = \frac{\mu_o m}{4\pi}\frac{(3cos\theta\hat{d} - \hat{m})}{d^3} \qquad (13)$$

The magnetic torque received by the pendulum can be written as:

$$\vec{T}_a = -B_{ao}m\frac{3sin2\theta}{4}\hat{x} \qquad (14)$$

where B_{ao} is the radial magnetic field of the magnetic disc at the distance of d at zero swing angle, i.e.,

$$B_{ao} = \frac{\mu_o m}{2\pi d^3} \qquad (15)$$

In addition to the magnetic torque, a net force is often generated between two pendulums. However, it can be easily proven in a vertically aligned pendulum array that the net force from the adjacent pendulums cancel each other but the torque doubles at each pendulum. Therefore, one may write the total torque received by each pendulum in the array in the following form:

$$\overrightarrow{\mathrm{T_a}} = -B_{ao} M_s V \frac{3sin2\theta}{4} \hat{x} \qquad (16)$$

We use the small angle approximation ($sin\theta \approx \theta$) to simplify the resulting differential equation. The pendulum equation with both external and self-biasing now becomes:

$$\frac{d^2\theta}{dt^2} = -\frac{\vec{T}_e + \vec{T}_a}{I} \approx -\frac{2M_s(B_e + 3B_{ao})}{\rho r^2}\theta \qquad (17)$$

The equation can be solved to give θ as

$$\theta(t) = \theta_{\max} \sin\left(\frac{1}{r}\sqrt{\frac{2M_s(B_e + 3B_{ao})}{\rho}}\, t\right) \qquad (18)$$

which yields the pendulum oscillation frequency as:

$$f = \frac{1}{2\pi r}\sqrt{\frac{2M_s(B_e + 3B_{ao})}{\rho}} \qquad (19)$$

where r is the radius of the cylinder, M_s is the magnetization density of the magnet in the pendulum, and ρ is the mass density of the magnet. It is to be noted that the frequency is inversely proportional to the radii of the magnets and directly proportional to the square root of the field strength and magnetization density. The desired frequency can be obtained by controlling these parameters. In our case, we have eliminated the need for a bulky external

magnet by relying only on the self-bias field. The magnetic potential energy is transferred to the kinetic energy of the pendulums back and forth while transmitting a dynamic field outward. Assuming no external bias and NdFeB magnets of radius 2 mm and with center to center distance of 4.8 mm, we can calculate the expected oscillation frequency or angular frequency of such a pendulum array as shown in Fig 2.3 from equation (19) as follows:

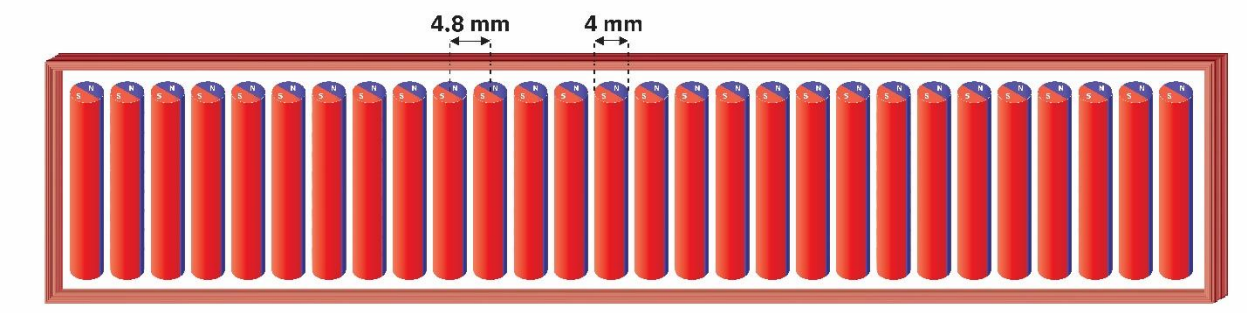

Figure 2.3: Schematic of a 28-element magnetic pendulum array consist of NdFeB magnets with 2 mm radius. Center to center distances between the magnets are 4.8 mm.

$$f = \frac{1}{2\pi r}\sqrt{\frac{6M_S B_{a_o}}{\rho}} \qquad (20)$$

We have $r = 2\,mm$, $\mu_o M_s = 1.4\,T$, $B_{a_o} = 2000\,G$ and $\rho = 7500\,kg/m^3$. Substituting these values, we get

$$f = 1062\,Hz \qquad (21)$$

Thus, although we are in the ULF range with a frequency of 1062 Hz, to scale up in frequency and reach transmission frequencies in the 3 kHz range, we need to reduce the radius of the magnets, the spacing between magnets or use stronger magnets to generate a higher self-bias field.

2.2 Q factor, Energy and Near field equations

2.2.1 Swing angle and Q factor

The major energy loss in the magnetic pendulum array is incurred because of friction between the magnets and bearings. Thus, friction limits the maximum Q factor and the efficiency that can be achieved in magnetic pendulum arrays. The quality factor limited by friction loss can be estimated as follows: The mechanical energy associated with a magnet with a radius r, moment of inertia I, and oscillating at a frequency Ω, can be written as

$$W_{ME} = \frac{1}{2} I\Omega^2 = \frac{1}{4}(\Omega r)^2 \rho V \qquad (22)$$

The friction loss by bearings per cycle is given by

$$W_{fr} = 4\mu F \theta_{max} r_b \qquad (23)$$

where μ is the co-efficient of friction, F is the residual force on the bearings due to the imbalance of the system, r_b is the radius of the bearing.

$$|\Omega| = \left|\frac{\partial\theta(t)}{\partial t}\right| \qquad (24)$$

with $\theta(t) = \theta_{max} \sin\left(\frac{1}{r}\sqrt{\frac{6M_s B_{a_o}}{\rho}}\, t\right)$

The Q factor then turns out be

$$Q = 2\pi \frac{W_{ME}}{W_{fr}} = \frac{3\pi M_s B_{a_o} \theta_{max} V}{4\mu F r_b} \qquad (25)$$

Thus, by reducing the bearing radius and friction loss further, and increasing the volume fraction of the magnets, magnetic pendulum arrays should be able achieve extremely high Q factors.

2.2.2 Near Field Radiation

The magnitude of the received magnetic field in the near field can be written as:

$$|B_{NF}| = \frac{2\mu_o M_s V}{4\pi d^3} sin\theta_{max} \quad (26)$$

Where $|B_{NF}|$ is the magnitude of the magnetic near field, V is the effective magnetic volume, d is the distance, and θ_{max} is the maximum swing angle of the pendulum. Based on this equation we can calculate the number of magnets required to construct the magnetic pendulum array for a given field at a certain distance. For Ex. To achieve a field of 1fT at 1km we need approximately 28 magnets of radius 2 mm and height 40 mm assuming a rotation angle $\theta_{max} = 20^o$. The array can be scaled with more magnets to increase the total volume to achieve higher fields.

2.2.3 Energy considerations

The energy associated with a pendulum array-based system is much smaller compared to spinning magnet systems. For Ex. Consider the 28-element pendulum array shown in Fig 2.3, the energy associated with each magnet is just 0.14 J and the energy density of each magnet is 296 kJ/m^3 which is smaller than the typical energy density of an NdFeB magnet of around 470 kJ/m^3. Even if the array is scaled up to consist of thousands of magnets the energy density remains the same for each magnet, but the total energy would increase. To achieve the fields comparable to that of spinning magnet and spinning magnet array described at the beginning of this chapter we would need approximately 2000 magnets of radius 2 mm and height 40 mm assuming a rotation angle $\theta_{max} = 20^o$. The total energy of such a system is 280 J which is much smaller than the energy of spinning magnet systems.

Chapter 3

Modelling and Simulation of Magnetic Pendulum Arrays

The magnetic pendulum array system consists of interactions between multiple physics such as Newton's laws and Maxwell's equations. It is important to accurately model such a system. For this purpose, we used ANSYS Maxwell 2D which is a 2D full wave low frequency solver. ANSYS Maxwell is Finite Element Method (FEM)-based electromagnetic field simulation software for the design and analysis of electromagnetic and electromechanical devices. ANSYS Maxwell can simulate transient magnetic (time domain) fields caused by permanent magnets as function of time. Rotational motion effects, eddy current losses, and frictional and damping losses can be included in the simulation. 2D simulations are performed using ANSYS Maxwell to validate our concept and understand the interactions between multiple physical laws and their effect on system design. The model consists of an array of 28 cylindrical, diametrically magnetized NdFeB magnets excited by a 55-turn coil as shown Fig 3.1. The coil is first excited with a gaussian wideband excitation to determine the resonant modes of the magnetic pendulum array. The torque experienced by magnet closest to the center of the array is plotted across frequency in Fig 3.2. The plot shows many distinct peaks corresponding to the different modes of the pendulum array. There is only one mode in which all the array elements oscillate in phase which is the mode at 1062 Hz. The magnetic pendulum array is then excited with this in phase mode frequency and the angular position of the edge magnets and the central magnet is plotted against time in Fig 3.3. We can observe that it is an in-phase mode in which the magnets are oscillating in-phase with respect to each other, and so it is the most efficient for ULF

transmission. It's also clear from Fig 3.3 that initially the magnets are not in phase and it takes time for the resonance to build up and the magnets to get aligned and oscillate in phase once the

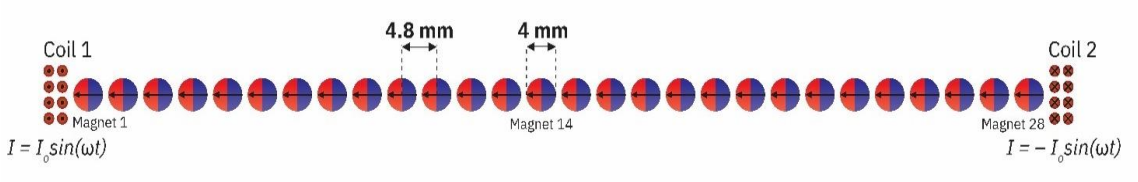

Figure 3.1: 2D cross sectional model of Magnetic Pendulum Array in ANSYS Maxwell.

resonance is established. Also, in the in-phase mode not all the magnets have the same angular amplitude. This inconsistency can be attributed to the fact that the magnets do not see the same bias field. The edge magnets see lower bias than the inner ones and hence has the lower amplitude. This is further clarified from the plot of magnetic field distribution shown in Fig 3.4.

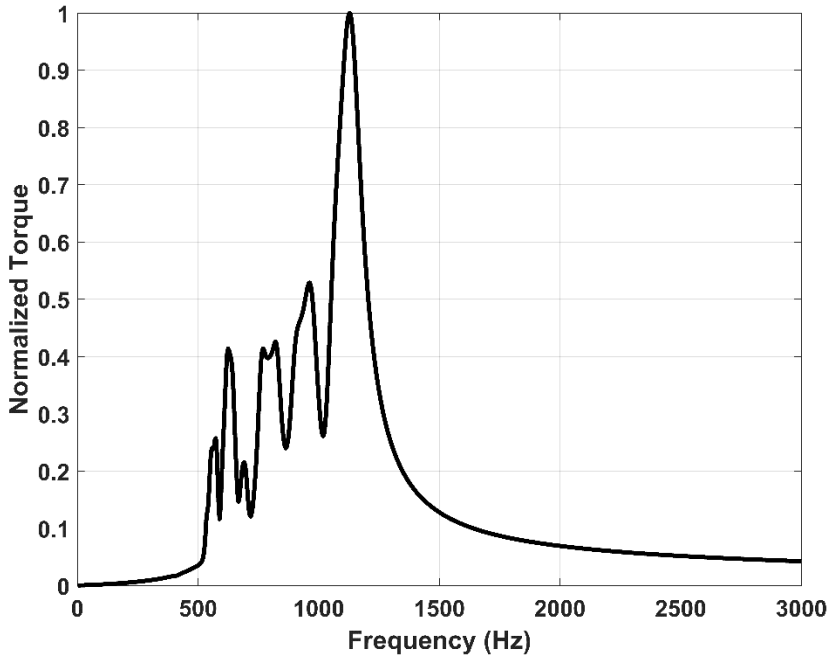

Figure 3.2: Torque on central magnet with wide band Gaussian excitation.

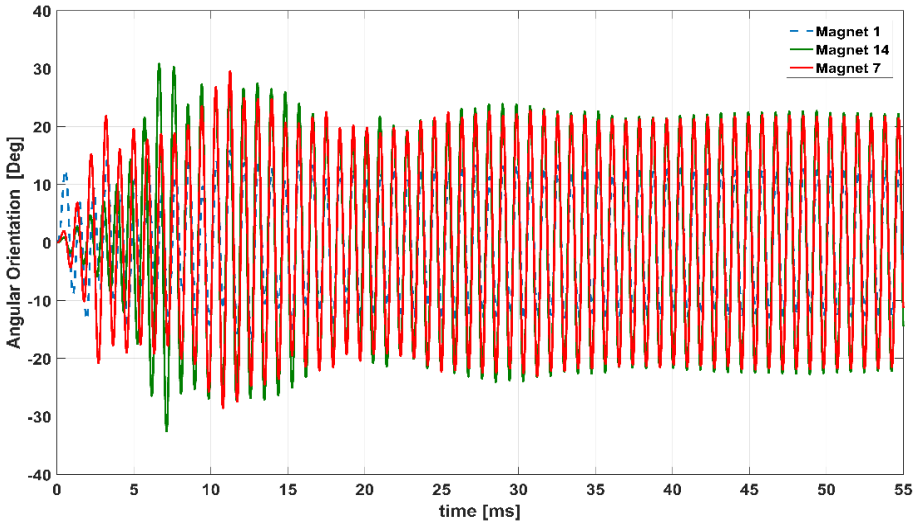

Figure 3.3: Simulated angular position of the magnets across time.

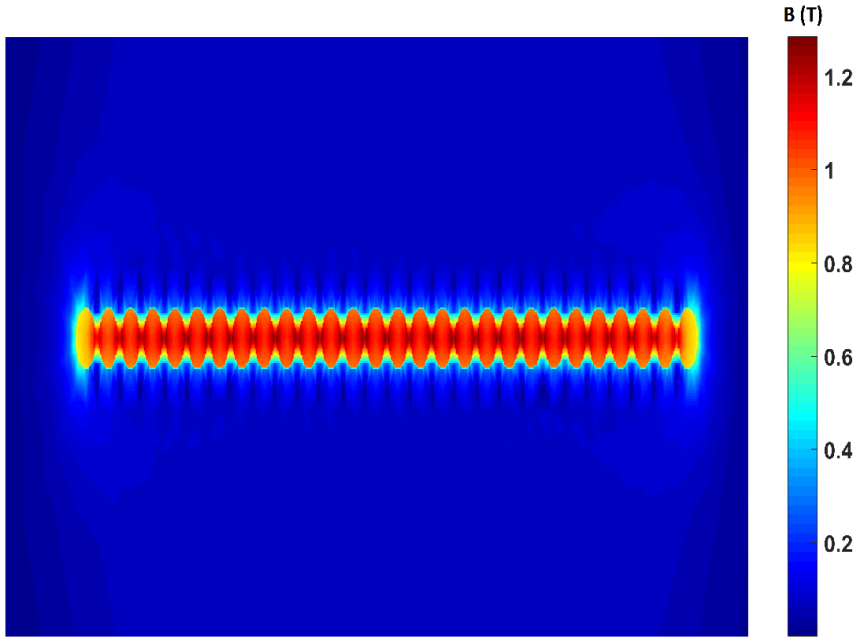

Figure 3.4: Magnetic field distribution. Observe the non-uniformity of the magnetic field across different magnets.

Chapter 4

Prototype measurements and Circuit modelling

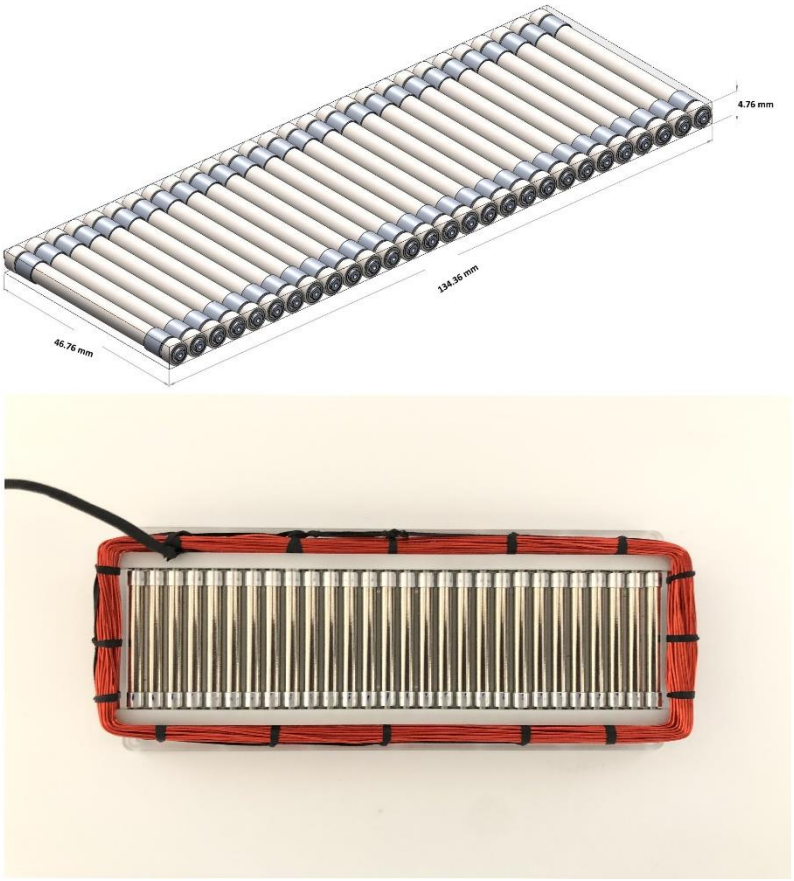

Figure 4.1: Magnetic pendulum array CAD model and prototype assembly.

A prototype of the magnetic pendulum array was fabricated and measured. The fabricated prototype is shown in Fig 4.1 along with the CAD model. The magnetic pendulum array consists of 28 pendulum elements suspended by stainless steel ball bearings in a plastic housing. Each pendulum element is comprised of a 40 mm long diametrically magnetized cylindrical NdFeB N55 magnet having a 4 mm radius and is supported by aluminum bearing adapter sleeves on

each end. The housing is made of plastic to prevent eddy current losses. A coil made of AWG26 copper wire with 55 turns is wrapped around the magnets to provide the excitation field. The sinusoidal input signal is generated from a signal generator and amplified using an audio power amplifier before being fed to the magnetic pendulum array. The receiver is a 45-turn loop antenna of radius 26 cm, and a spectrum analyzer is used to observe the received signal. The measurement setup is diagrammatically represented in Fig 4.2.

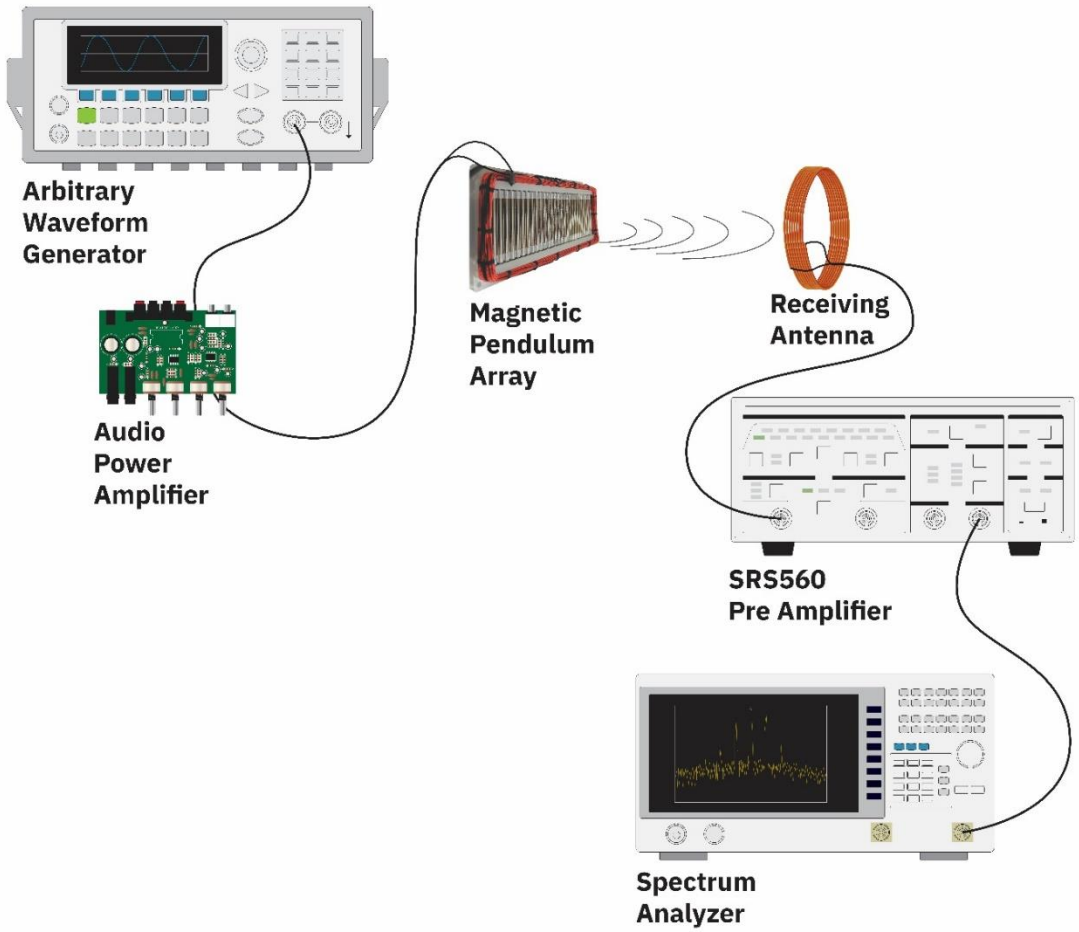

Figure 4.2: Schematic of the measurement setup.

4.1 Near field transmission measurements

The transmission efficiency of the magnetic pendulum array as compared to a bare coil is plotted in Fig 4.3. In general, the efficiency of coupling increases with the frequency for both cases as a greater quality factor is obtained for the coil at higher frequency which helps to increase the power coupled through nearfield. The efficiency is maximum in the in-phase mode at 1031 Hz, as expected. The transmission efficiency of magnetic pendulum array is about 7 dB higher than a bare coil at 1031 Hz. The spiking of the efficiency at resonance can be explained by the fact that, more power is coupled to the pendulum array versus that is coupled to the coil. A range test was performed at the resonance frequency, results of which are shown in Fig 4.4. The tests were performed in free space environment at the UCLA Intramural field. The transmitted power into the coil loaded with the magnetic pendulum array are 0.6 W and 1.9 W for Fig 4.4 a, b, respectively. The measured results are compared with the analytical results derived from the near field equation shown in Eq 26 of Chapter 2 and a good agreement is observed. A range of 25 m and 30 m were obtained on the receiver end for 0.6 W and 1.9 W input powers as shown in Fig 4.4. A data transmission test was performed at 2 bit per second (bps) modulation rate with On-Off Keying (OOK) modulation scheme. The test was performed indoors with the receiver at 3 m from transmitter. The received spectrogram is shown in Fig 4.5 (a) and the received spectrum is shown in Fig 4.5 (b). Even though the data rate is small, it demonstrates that data can be successfully transmitted using magnetic pendulum arrays. At higher Q factors Direct Antenna Modulation (DAM) can be implemented with more complex modulation schemes such as Binary Frequency Shift Keying (BFSK) to achieve higher data rates. This would be demonstrated for the 2D pendulum array prototype.

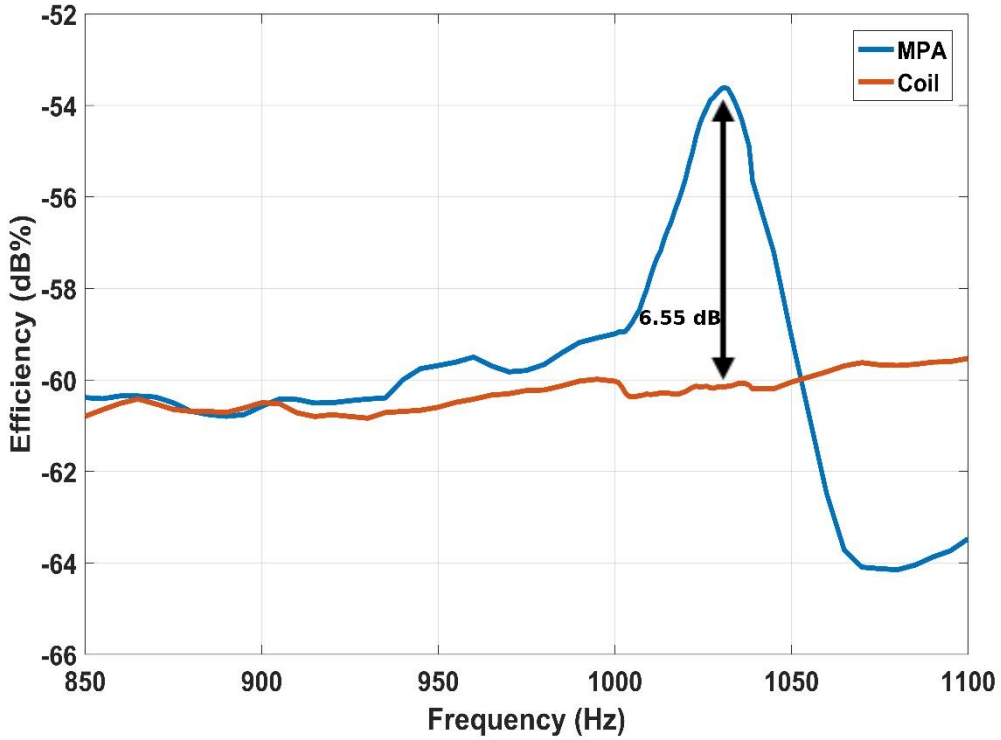

Figure 4.3: Transmission efficiency of magnetic pendulum array compared to that of a bare coil.

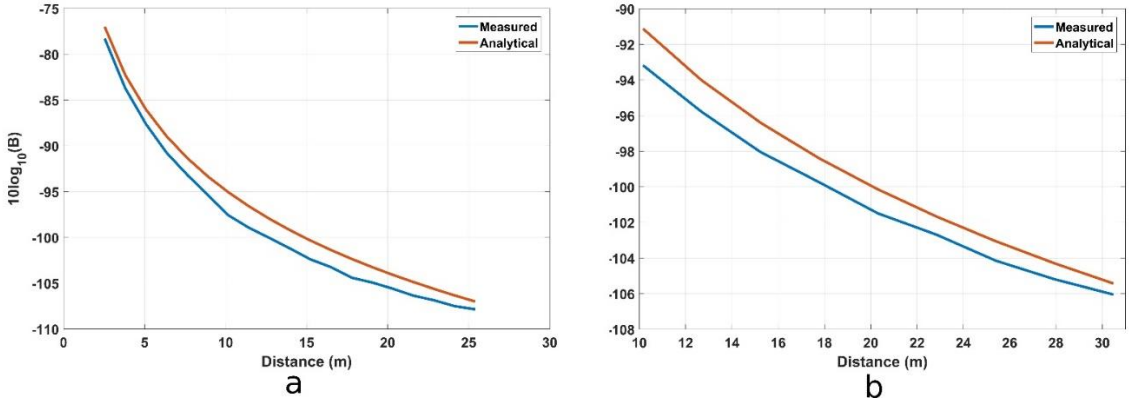

Figure 4.4: Received field vs distance using a 45-turn loop antenna as receiver. Measurements were done at 1031 Hz. Input power to the coils are (a) 0.6 W (b) 1.9 W.

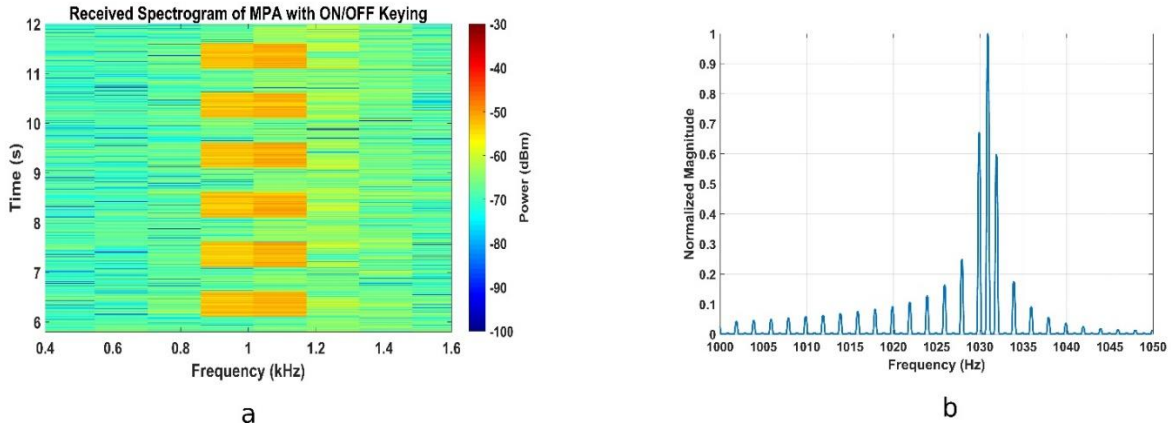

Figure 4.5: Data transmission test with OOK (a). Received signal spectrogram (b). Received signal spectrum.

4.2 Equivalent circuit Model and Impedance measurements

In this section, we develop an equivalent circuit model based on the physics of coupling between the coil and magnets. Circuit models can help us understand the system in an intuitive way and are great tools to quickly verify some of the properties of the system. It is common to use a distributed element model in microwave engineering to model transmission lines and other periodic structures. But a lumped element circuit model is justified here as the wavelengths are very long compared to the dimensions of the elements. The magnetic pendulum array can be modeled as a parallel RLC circuit, as shown in Fig 4.6 (a). The resistance of the coil is modeled as R_c and the inductance of the coil is modeled as L_c. The resistance R_p represents mainly the friction in the bearings. The capacitor C_p represents the kinetic energy of the pendulum as the oscillatory motion of the pendulum generates Electro Motive Force (EMF), and the inductance L_p represents the magnetic potential energy stored in the flux associated with the pendulum. The magnetic field from the coil that turns the magnets can be modeled as the current in the circuit, and the Electro-Motive Force (EMF) generated in the coil by the oscillating

magnets can be modeled as voltage. Both, a series and a parallel resonant mode can be observed in the pendulum array. The parallel resonant mode ω_p can be written as

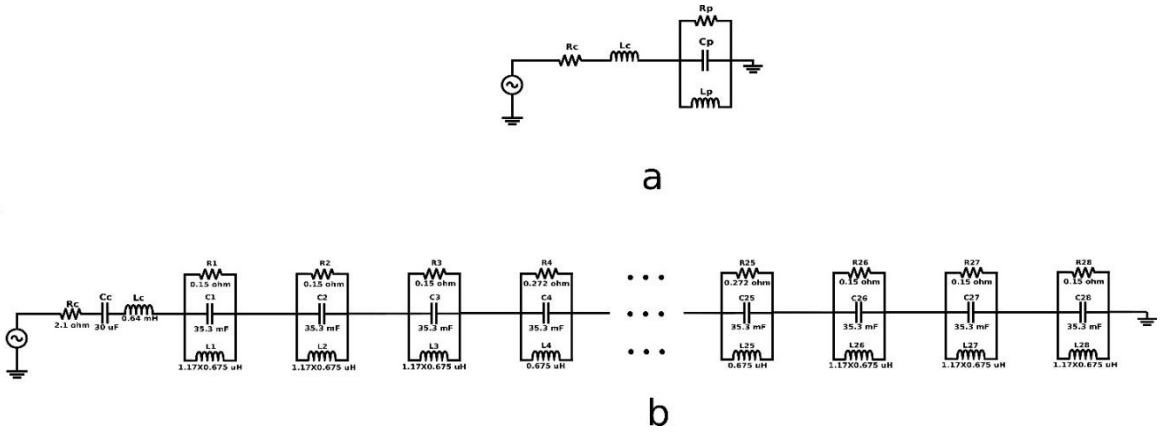

Figure 4.6: Equivalent circuit model for Magnetic Pendulum Array (a). Equivalent circuit model for one element (b). Equivalent circuit model for 28-element Magnetic Pendulum Array.

$$\omega_p = \frac{1}{L_p C_p} \tag{1}$$

At resonance, the imaginary part of the sum of the impedances can be equated to zero as

$$Imag\left(\mathrm{j}\omega_s L_c + \frac{1}{\frac{1}{j\omega_s L_p} + j\omega_s C_p + \frac{1}{R_p}}\right) = 0 \tag{2}$$

Assuming the system Q factor to be high, we can neglect the frictional and mechanical losses and ignore the $1/R_p$ term. Further simplification for the series resonance ω_s leads to

$$\omega_s = \sqrt{\frac{L_C + L_P}{L_C L_P C_P}} \tag{3}$$

The model can be extended to an array by cascading the single element to include the effect of non-uniform bias on the magnets at both ends, as shown in Fig 4.6 (b). Observe that the

inductance on the edge elements is higher than in the middle accounting for non-uniform bias and resistance is much lower on the edges, indicating a higher loss and lower Q. Capacitor C_c is used to compensate for the inductance of the coil and match the impedance. For the 28-element magnetic pendulum array as shown in Fig 4.1. the circuit parameters are calculated as follows,

$$R_c = 2.1\ \Omega, C_c = 30\ \mu\text{F}, L_c = 0.64\ \text{mH},$$
$$R_1 = R_2 = R_3 = R_{26} = R_{27} = R_{28} = 0.15\ \Omega,\ \ R_4 = R_5 = \cdots = R_{25} = 0.272\ \Omega$$
$$C_1 = C_2 = \cdots = C_{28} = 35.3\ \text{mF}$$
$$L_1 = L_2 = L_3 = L_{26} = L_{27} = L_{28} = 0.79\ \mu H,\ \ L_4 = L_5 = \cdots = L_{25} = 0.675\ \mu H$$

When the impedance of the circuit is plotted across frequency which is presented in the following section, sharp resonance is observed at around 1031 Hz consistent with our predicted value of resonance frequency. The circuit model clearly demonstrates the advantage of using mechanical antennas and the system resonance for ULF transmission. At resonance, the current through the coil (represented by R_c and L_c) is significantly reduced, thereby reducing the ohmic losses present in the system. Such reduction in current is not possible in conventional antennas and therefore higher efficiencies can be achieved in the mechanical antennas as compared to conventional antennas. The circuit model is not a complete description of the system as it does not consider the time varying nature of the flux and the non-linearities inherently present in this system. But the circuit model is still of great help in visualizing the system, verifying the predicted values of the resonance frequency, and estimating the Q factor of the system. The Q can be estimated as follows:

$$Q = R\sqrt{\frac{C}{L}} = 0.272\sqrt{\frac{35.3\times10^{-3}}{0.675\times10^{-6}}} = 62.2 \qquad (4)$$

Fig 4.7 shows the input impedance of the pendulum array prototype, coil and the circuit model plotted across frequency. The peaking of the input impedance indicates a greater portion of the

input power is coupled to the pendulum system while the power consumption caused by the ohmic loss of coil is relatively reduced. Note that not all the modes were predicted by the circuit model due to the fact the mutual coupling among the pendulum elements are not included in the model demonstrating the superiority and completeness of the full wave model. The estimated Q factor at the in-phase mode is around 62.2 as previously demonstrated using the circuit model. To our knowledge, this is the first time such a high Q factor has been achieved in a mechanical antenna system using magnetic dipoles at ULF, demonstrating the potential of magnetic pendulum arrays for efficient ULF transmission.

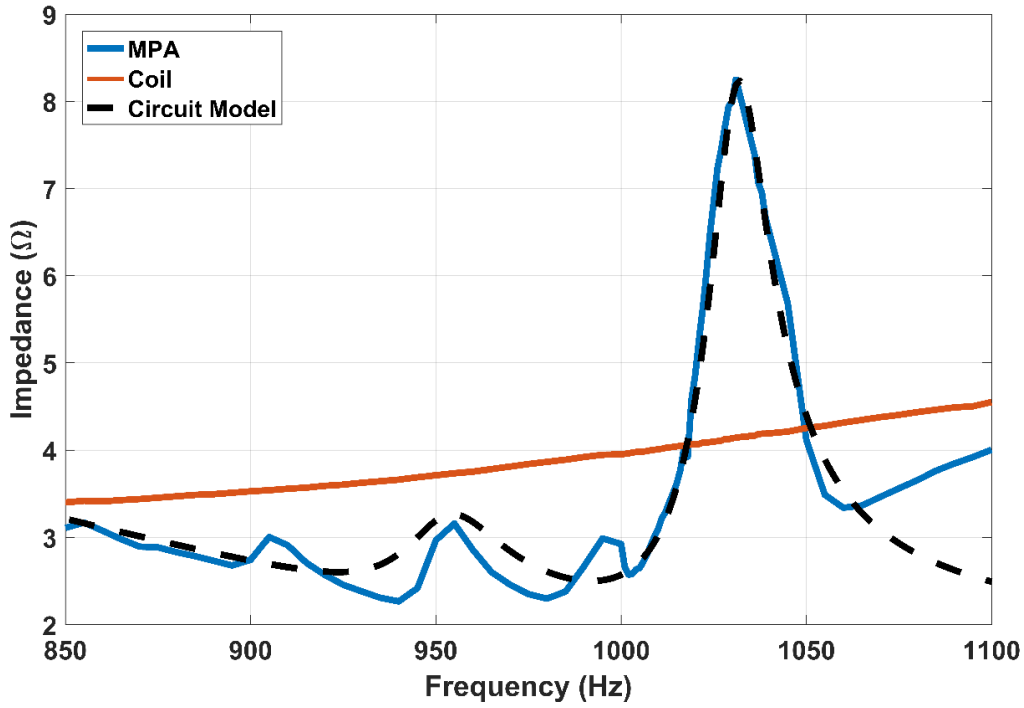

Figure 4.7: Measured impedance and predicted impedance from circuit model versus frequency.

4.3 Effect of non-uniformity of pendulum elements on system performance

The circuit model can also be used to study the effect of non-uniformity and random variations in the pendulum elements on system performance. Random variations in the radii of magnets results in different resonant frequency for each magnet because the resonant frequency is inversely proportional to the radius of the magnets as demonstrated in Eq 20 of Chapter 2. This effect has been studied by introducing random variations in the circuit element parameters of the circuit model shown in Fig. 4.6 (b). The tolerance on the radius of the magnets specified by the vendor is $\pm 0.05\, mm$. We vary the radius of the magnets as a random sample of a normal distribution based on the vendor specified tolerance thus varying the circuit parameters in the model. Though each resonator in a non-uniform array is at a slightly different frequency, together they will be excited to oscillate at an identical frequency, but with a reduced system quality factor that can be observed from the input impedance of the equivalent circuit model. The effect of the random variations and non-idealities can be quantified by the ratio of the impedance for the uniform and the non-uniform array across different Q factors. The results of such a study are shown in Fig. 4.8. The overall impact on the system impedance is minor for pendulum arrays with a Q factor of few hundreds. We observe that the effect becomes more pronounced as the system Q factor increases. Thus, we conclude that for our prototypes with Q factor of less than 100 the effect of non-uniformities in the pendulum elements is not significant and can be ignored.

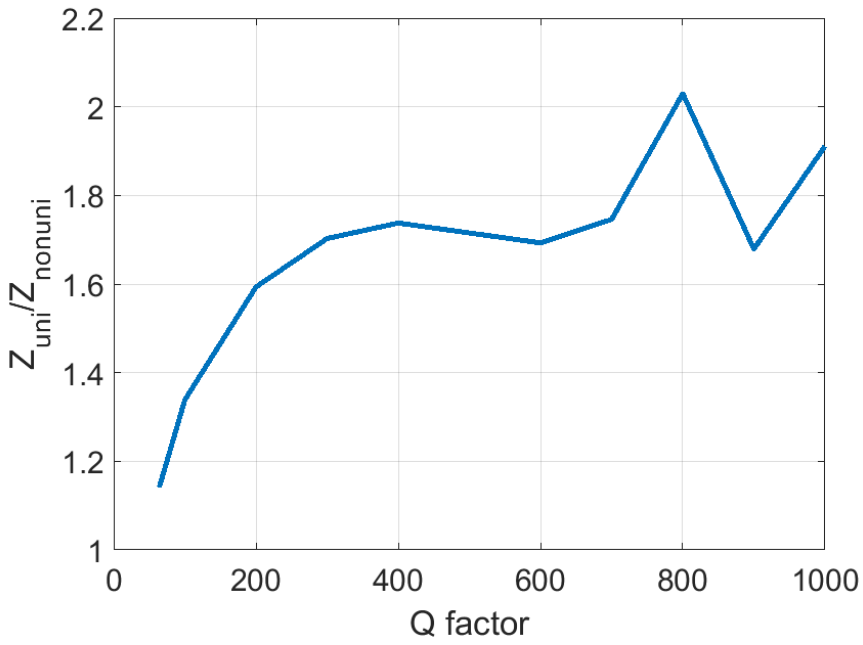

Figure 4.8: Effect of random variations in pendulum elements on system performance.

Chapter 5

Stacked Magnetic Pendulum Arrays

5.1 2D stacked pendulum arrays

In this case, instead of arranging the magnets along just a row, we stack the magnets both along the row and column leading to 2D stacked magnetic pendulum arrays. The scaling of the MPA in the direction out of the equilibrium magnetization plane exploits the linkage of the flux and mutual coupling among the magnets to achieve the following advantages. It can lead to higher transmitted field as we now have more magnetic volume and higher Q factors. The second advantage is that a 2D stacked structure will have higher inductance as compared to the RF coil, thus making it efficient to implement Direct Antenna Modulation (DAM) for transmitting information. But it is to be noted that the resonant frequency of 2D stacked pendulum arrays can be much lower as compared to 1D magnetic pendulum arrays. There can be two configurations for stacked pendulum array. In the parallel configuration the magnets in each row have the same orientation with respect to the other rows. In the anti-parallel configuration magnets in each row have the opposite pole arrangement compared to the adjacent rows. We study the anti-parallel configuration in this work as it is a more stable configuration and easier to build and assemble. In the following sections we describe the resonant frequency calculation for 2D stacked arrays, its construction and measurements.

5.1.1 2-D MPA resonant frequency calculation

We follow the same approach as described previously for 1D arrays to calculate the resonant frequency of 2D arrays. For each magnet in the lattice (except the edge magnets), there are four magnets around as shown in Fig 5.1. Two magnets placed at a distance *d* horizontally and two others with the distance of *h* vertically. In equilibrium, all magnets are oriented horizontally as horizontal torque is dominant (d<h). However, when the time variant magnetic flux by the solenoid comes in, the additional torque will force the magnets to oscillate within $+\theta_{max}/-\theta_{max}$ around their equilibrium angle ($\theta_{equ.} \approx 0$) as shown in Fig 5.2.

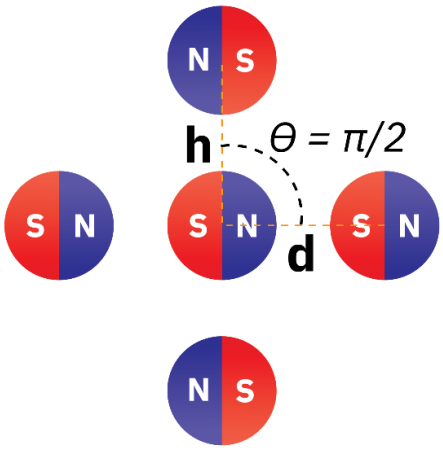

Figure 5.1: Each magnet consists of 4 nearest neighbors. Two along the horizontal and two along the vertical.

We can write the equation of motion for the magnet in the center as

$$-T = I\frac{d^2\theta}{dt^2} + B\frac{d\theta}{dt} + k\theta \qquad (1)$$

Where T is the restoring torque, I is the moment of Inertia of the magnets, B is the co-efficient of friction and k is the torsional constant.

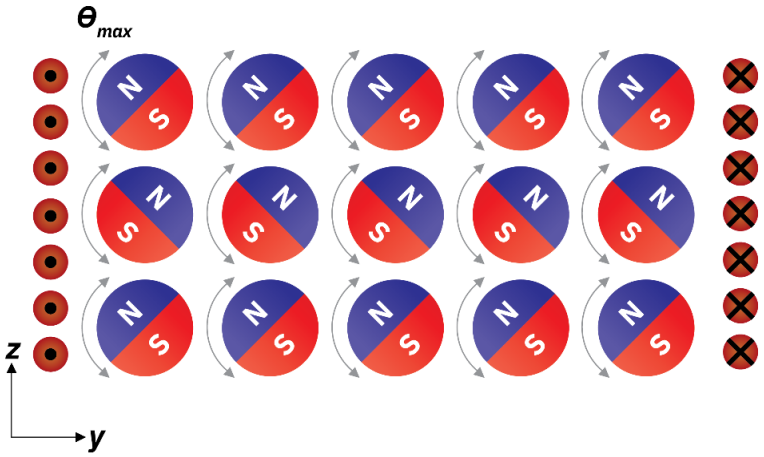

Figure 5.2: Rotation of the magnets around equilibrium position.

We ignore k as we don't have spring torsion in our system and assume there is no friction present. The torque between two cylindrical magnets has been derived in Appendix A. The equation can be written as

$$-\left(2\times\frac{\pi\mu_0 M_S^2 r^4 w\sin(2\theta)}{2h^2}-2\times\frac{\pi\mu_0 M_S^2 r^4 w\sin\left(2\left(\frac{\pi}{2}-\theta\right)\right)}{2d^2}\right)=I\frac{d^2\theta}{dt^2} \qquad (2)$$

Where M_s is the magnetization of the magnets, r is the radius of the magnets, w is the height of the magnets. We can write the Moment of Inertia I as $\frac{1}{2}\rho V r^2$ where ρ is the density and V is volume of the magnet. We use the small angle approximation and assume $sin\theta \approx \theta$. The equation can be simplified as follows:

$$-\pi\mu_o M_S^2 r^4 w\left(\frac{1}{h^2}-\frac{1}{d^2}\right)2\theta=\frac{1}{2}\rho\pi r^2 w r^2\frac{d^2\theta}{dt^2} \qquad (3)$$

$$-\frac{4\mu_o M_s^2}{\rho}\left(\frac{1}{h^2}-\frac{1}{d^2}\right)\theta=\frac{d^2\theta}{dt^2} \quad (4)$$

We can write solution of the above differential equation as

$$\theta(t)=\theta_m \sin(2\pi f t) \quad (5)$$

Where $f=\frac{\omega}{2\pi}=\frac{1}{2\pi}\sqrt{\frac{4\mu_o M_s^2}{\rho}\left(\frac{1}{h^2}-\frac{1}{d^2}\right)}$

Assuming $d=4.8\,mm$ and $h=1.5d=7.2\,mm$, we can calculate the resonant frequency of a 2D array as

$$f=713\,Hz \quad (6)$$

As can be seen this is smaller than the frequency derived for the 1D pendulum array.

5.1.2 Design and construction of 5 X 11 Magnetic Pendulum Array with antiparallel configuration

Based on the above results for resonant frequency, we propose a 5X11 Magnetic Pendulum Array consisting of 55 magnets arranged in 11 rows with 5 magnets in each row. In this proposed prototype the magnets in each row have the opposite orientation with respect to the adjacent

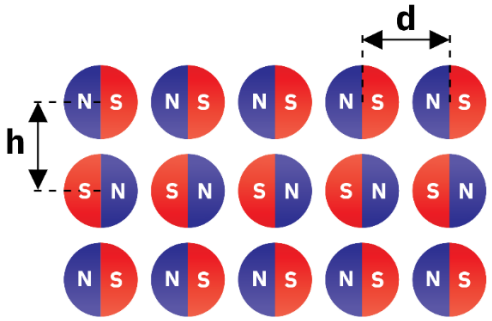

Figure 5.3: Anti-parallel configuration of stacked pendulum array.

rows as shown in Fig 5.3. A solenoid consisting of 100 turns of 22 AWG copper wire is used to excite the structure and enforce the magnets to oscillate around the equilibrium position. The horizontal and vertical spacing between the magnets are $d = 4.8\,mm$ and $h = 7.2\,mm$ respectively. Stationary bar magnets are placed on both the sides to reduce the edge magnet effect. This has the following benefits. It increases the angle of oscillation of the edge magnets which in turn increases the transmitted magnetic field. It balances the force on the edge magnets and increases the overall quality factor of the system. It also increases the overall inductance of the system thereby aiding in implementing an efficient Direct Antenna Modulation (DAM) scheme. Fig 5.4 shows the cross section of the proposed prototype and the fabricated model.

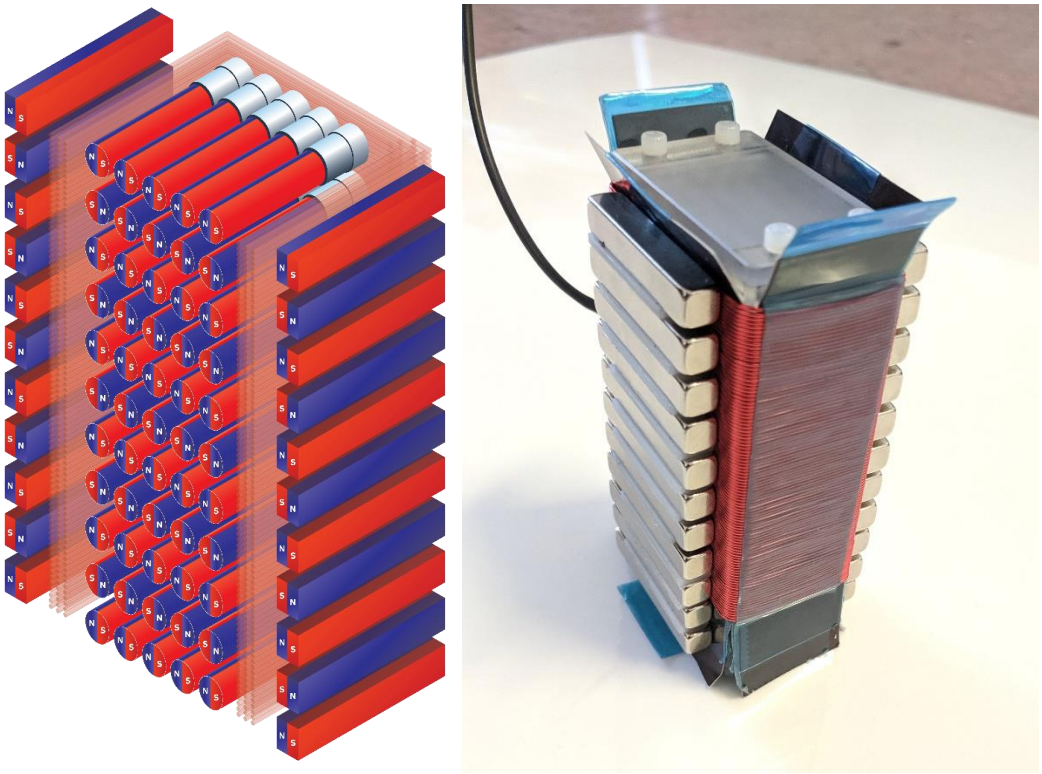

Figure 5.4: Proposed 5X11 array prototype cross section along with the fabricated model.

5.2 Measured results

A measurement setup like the one show in Fig 4.2 is used to measure the performance of the stacked magnetic pendulum arrays. We first present the near field transmission measurements and then the impedance and efficiency measurements along with the circuit model.

5.2.1 Near field transmission measurements

Fig 5.5. shows the received field measured in free space environment at the UCLA Intramural field plotted vs the distance. The measurement was done at the resonance frequency of the prototype determined to be 727 Hz with input power to the coil as 2W. A range of 30 m was achieved. The measured results were compared with the analytical value derived using Eq 26 of chapter 2.

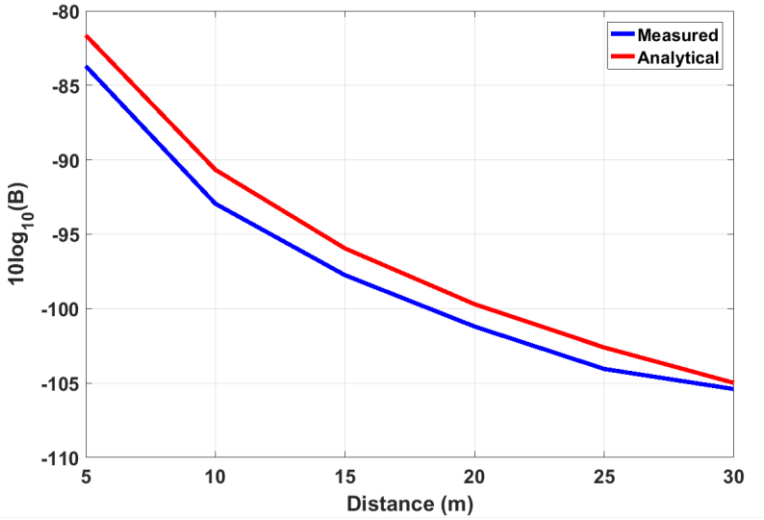

Figure 5.5: Received field vs distance using a 45-turn loop antenna as receiver.

The measured results match well with the analytical values. Another point to note is that the field values obtained are approximately twice as that obtained from the 28-element 1D pendulum array as expected.

5.2.2 Circuit model, impedance and efficiency measurements

An equivalent circuit model is developed for the stacked pendulum array based on the same principles described in Section 4.2, Chapter 4. Each row of 5 magnets is modeled as a parallel RLC circuit. The circuit model consists of 11 parallel RLC circuits in series with each other as our prototype consists of 11 rows as shown in Fig 5.6.

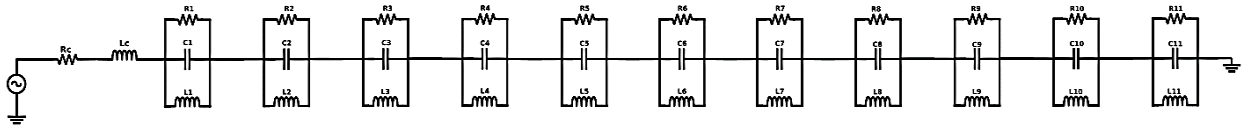

Figure 5.6: Equivalent circuit model of 5X11 Magnetic Pendulum Array prototype.

The circuit parameters are calculated as follows:

$$R_c = 1.37\ \Omega, L_c = 0.22\ \text{mH},$$
$$R_1 = R_{11} = 2.4\ \Omega, R_2 = R_{10} = 3.26\ \Omega, R_3 = R_9 = 4.23\ \Omega, R_4 = R_8 = 6.04\ \Omega, \mathrm{R}_5 = R_7 = 6.46\ \Omega, R_6 = 8.18\ \Omega$$
$$C_1 = C_{11} = 8.6\ \text{mF}, C_2 = C_{10} = 6.3\ \text{mF}, C_3 = C_9 = 4.9\ \text{mF}, C_4 = C_8 = 3.4\ \text{mF}, C_5 = C_7 = 3.2\ \text{mF}, \mathrm{C}_6 = 2.5\ mF$$
$$L_1 = L_{11} = 5.58\ \mu H, L_2 = L_{10} = 7.56\ \mu H, L_3 = L_9 = 9.83\ \mu H, L_4 = L_8 = 14.02\ \mu H, L_5 = L_7 = 15\ \mu H, L_6 = 19\ \mu H$$

When the impedance of the circuit is plotted across frequency as shown in Fig 5.7., sharp peak is observed at the resonance frequency of 727 Hz which is very close with our predicted value of resonance frequency. The Q from the circuit model can be estimated as follows:

$$Q = R\sqrt{\frac{C}{L}} = 8.18\sqrt{\frac{2.5\times10^{-3}}{19\times10^{-6}}} = 94 \qquad (7)$$

Observe that the peak impedance and the Q factor is higher than what we calculated for the 1D array. This is as expected since we hypothesize that the 2D architecture would lead to higher Q factors because of the flux linkage and coupling between the magnets along the horizontal and vertical directions. The circuit model can also be used to estimate the efficiency by noting the

fact that the received power is proportional to the square of the voltage on the transmitter. Thus, for the MPA we can write the efficiency η_{MPA} as

$$\eta_{MPA} = \frac{|V_{MPA}|^2}{Real(P_{inMPA})} = \frac{(R_{MPA}I)^2}{(R_{MPA}+R_c)I^2} = L_{MPA}Q_{MPA}\omega \quad (8)$$

Where I is the current through the transmitter, R_{MPA} and L_{MPA} refer to the total resistance and inductance of the MPA respectively and Q_{MPA} is the Quality factor of the MPA. V_{MPA} is the voltage on L_c in the circuit model of Fig 5.6. Similarly, we can write the efficiency η_{coil} of just the coil with a Q factor of Q_c as

$$\eta_{coil} = \frac{|V_{coil}|^2}{Real(P_{incoil})} = \frac{(\omega L_c I)^2}{(R_c^2 I^2)} = L_c Q_c \omega \quad (9)$$

Where V_{coil} is the voltage on L_c without the MPA. By taking the ratio of the efficiencies we can gather further insight into sizing the coil to maximize the efficiency of MPA

$$\frac{\eta_{MPA}}{\eta_{coil}} = \frac{L_{MPA}Q_{MPA}}{L_c Q_c} \quad (10)$$

From Eq 10 we can see that we need to size the coil for the minimum inductance possible to maximize the efficiency of the MPA. It is to be noted that with the circuit parameters and Q calculated earlier we observe that the efficiency ratio is about 18 dB. We then measure the efficiency of pendulum array compared to a coil of same dimensions. The efficiency is calculated as the difference of the received power and the input power in logarithmic scale. The receiver is coil placed at 40 cm from the transmitter. While measuring the efficiency of the transmitter coil, it is matched with a capacitance to compensate for the imaginary part of the impedance.

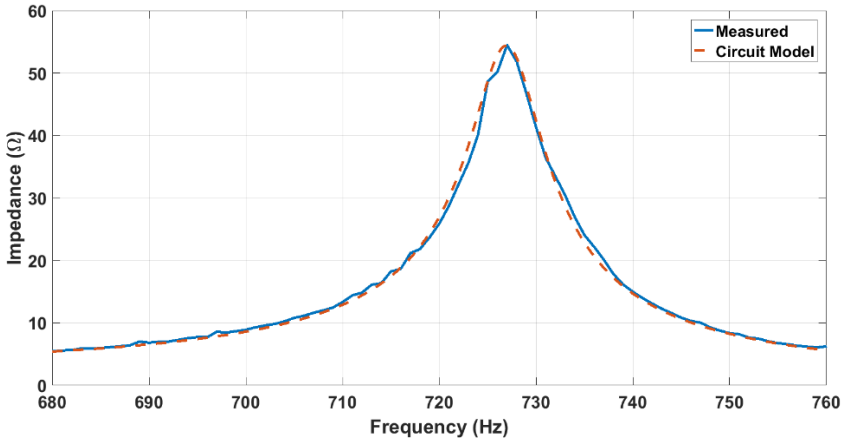

Figure 5.7: Measured impedance vs frequency.

About 18 dB of improvement in efficiency is observed at the resonance frequency as shown in Fig 5.8 which is much higher than what was achieved using the 1D arrays proving the superiority of stacked pendulum arrays. It also matches with the value predicted by the circuit model.

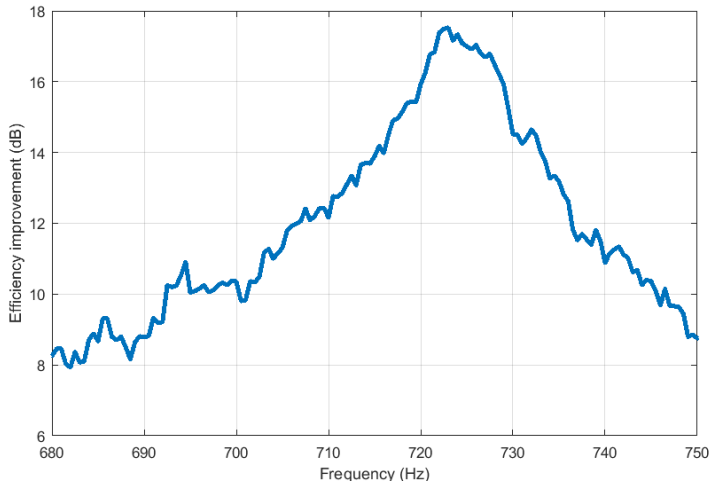

Figure 5.8: Efficiency improvement of a pendulum array as compared to a coil.

Chapter 6

Direct Antenna Modulation (DAM): Implementation and Measurements

6.1. Concept of Direct Antenna Modulation (DAM)

In this section we illustrate the concept of Direct Antenna Modulation (DAM) using a switched small loop as shown in Fig 6.1. The input impedance of the loop is inductive as it is electrically small. A capacitor C is inserted in series to form resonance. The quality factor of such a system is very high if the losses are minimized resulting in very narrow bandwidth. To perform DAM a switch S2 is inserted in series to short circuit the current flow while the current through the loop reaches to its maximum, as shown in figure 6.1(a). This helps to maintain the stored inductive energy in the near field while stopping the radiation caused by an oscillating current. When radiation is needed, one can turn on the switch and the loop inductor will start to release its inductive energy into the matching capacitor and create oscillating current and its radiation without delay, as shown in figure 6.1(b). The switch S1 in series with the capacitor is to prevent the current spike caused by switching off the residue voltage in the capacitor. It is found that the modulation bandwidth of the radiation scan be as fast as the carrier frequency [22]. In the next section we describe how the DAM scheme has been implemented on magnetic pendulum arrays along with the circuit model for the DAM scheme.

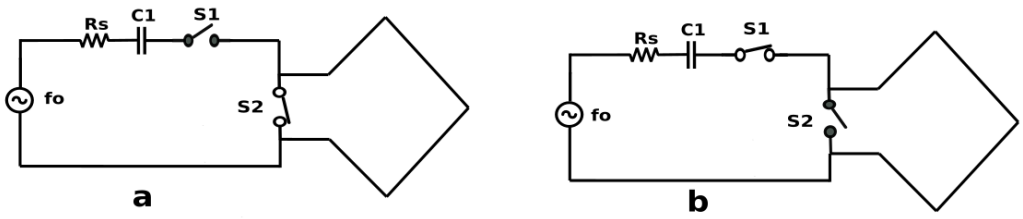

Figure 6.1: Illustration of DAM with switched electrically small loop.

(a) Storage Mode (b) Radiation Mode

6.2. Implementation of DAM scheme on 5X11 stacked pendulum array

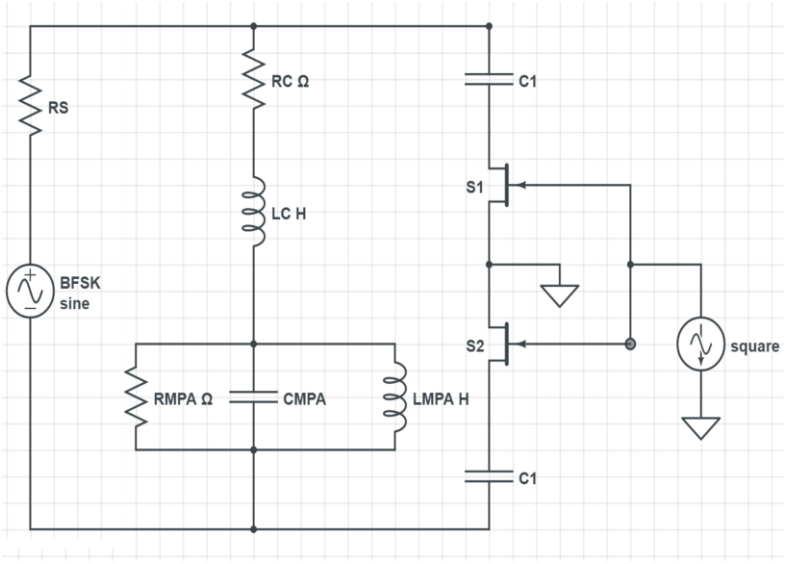

Figure 6.2: Equivalent circuit model of DAM implementation on 5X11 stacked pendulum array.

The DAM-MPA system consists of pendulum array loaded with a capacitance and integrated with GaN semiconductor switches consisting of a pair of transistors that are placed in a complementary fashion. The system is designed to transmit a Binary-Frequency Shift Keying (BFSK) signal with a data rate of 18 bps. The equivalent circuit model of DAM implementation

on 5X11 stacked pendulum array is illustrated in Fig 6.2. The pendulum array is represented by a single equivalent parallel RLC circuit with $R_{MPA}, C_{MPA}\ and\ L_{MPA}$ resonating at frequency $f_1 = 735\ Hz$. R_C and L_c represent the solenoid resistance and inductance respectively. Capacitance C_1 and C_2 is added in parallel forcing the circuit to resonate at frequency $f_2 = 697\ Hz$. Transistors S_1 and S_2 are used to efficiently and passively switch between two chosen carrier frequencies f_1 and f_2. The design incorporates a pair of GaN transistors that act as switches in a complimentary fashion to increase isolation between radiated signal and the switch control path to prevent loading effects between transistor and the pendulum array. To preserve near field energy stored in the antenna system, it was proposed that the switching action happens at the maximum RF voltage moment for electrically small dipoles [24], [25] and at the maximum current moment for electrically small loops [26]. In our system the switching happens at maximum current on the inductor L_{MPA}, i.e. minimum input voltage as shown in Fig 6.3. We also ensure that the input voltage and current are in phase in both the ON state (697 Hz) and the OFF state (735 Hz). It is also important to note that the frequencies f_1 and f_2 should be sufficiently far from each other such that there is not ambiguity in the received spectrum to demodulate signal. If the difference between the frequencies is very high the capacitance will reduce the Q factor of the system by decreasing the impedance. Hence, we choose the minimum frequency difference such that the received signal can be demodulated without any ambiguity and the Q factor of the system is maintained sufficiently high. We can write the switching frequency f_{sw} as

$$f_{sw} = 1/(T_{on} + T_{off}) \qquad (1)$$

We have $T_{on} = \frac{38}{f_{on}}$ and $T_{off} = \frac{38}{f_{off}}$ which gives us a switching frequency $f_{sw} = 9\ Hz$ i.e. we can achieve a data rate of 18bps. A simple PCB is fabricated to accommodate the switching transistors and the capacitance as shown in Fig 6.4.

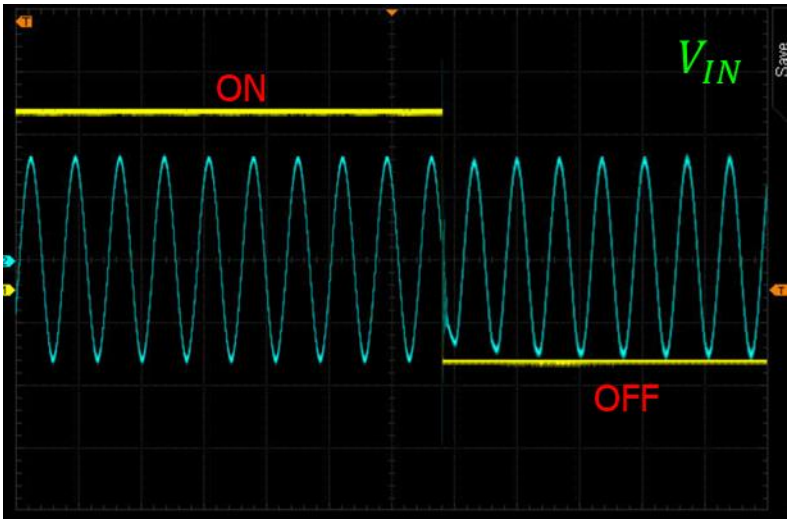

Figure 6.3: Switching at zero voltage moment (Maximum current on L_{MPA})

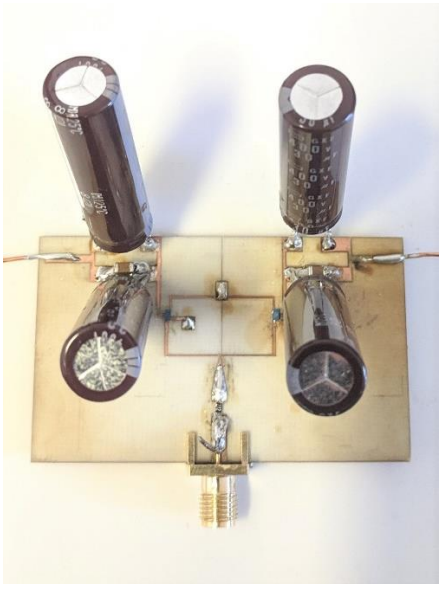

Figure 6.4: Fabricated PCB with switches and Capacitors.

6.2.1 Measured Results

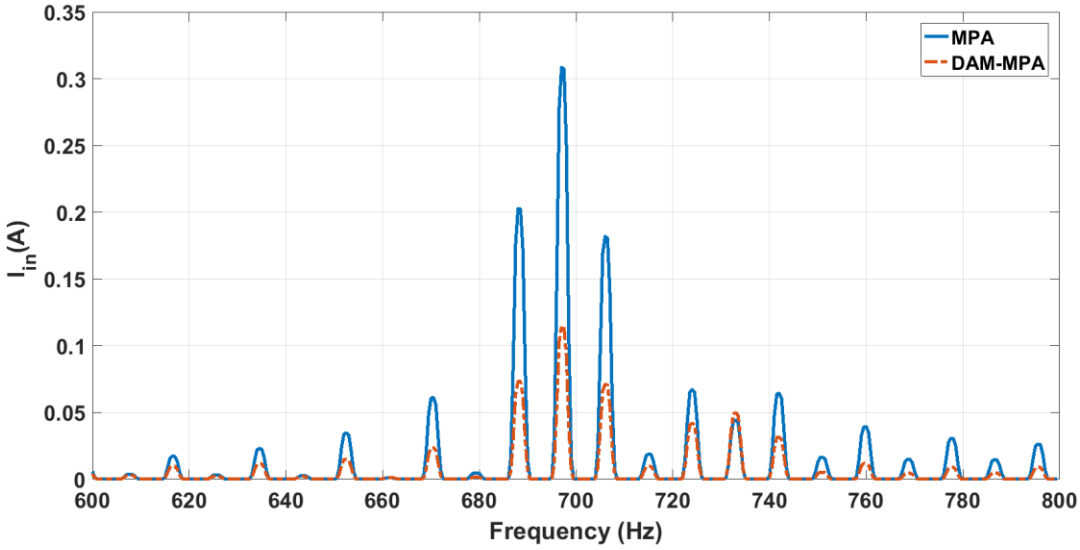

Figure 6.5: Input current vs frequency for DAM-MPA and MPA.

The input current to the MPA system was measured with and without the DAM scheme and plotted across frequency as shown in Fig 6.5. Input current at 697 Hz decreases by 8.6 dB in DAM case. It is to be noted that we apply a constant voltage source through an amplifier and hence the change in the resonance is reflected only in the current. This verifies the higher efficiency of Directly Modulated MPA over wider bandwidth in comparison to just the MPA transmitting a BFSK signal. The received voltage for MPA and DAM-MPA is same for most of the frequencies or DAM is higher in some frequency harmonics as seen in Fig 6.6. This shows that with small input power to the antenna in the DAM case we still get the same transmitted power thus proving the efficiency improvement in using a DAM scheme for BFSK transmission.

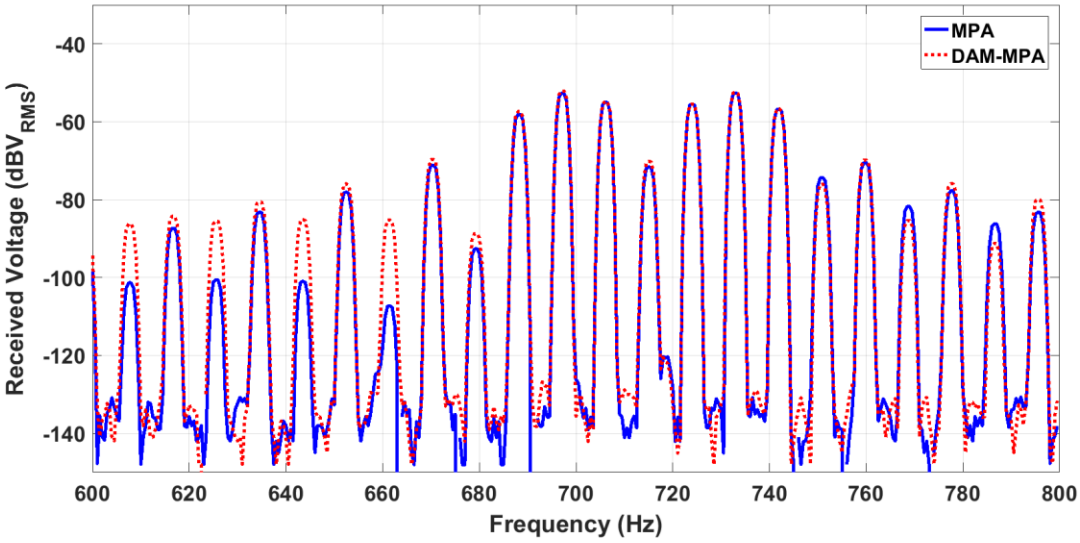

Figure 6.6: Received Voltage vs frequency for DAM-MPA and MPA.

Chapter 7

Summary

7.1 Conclusion

In this dissertation, we proposed and successfully demonstrated an electro-mechanical transmitter for efficient ULF transmission. The innovative design of 1D and 2D stacked magnetic pendulum arrays having high Q factors which utilizes mechanical resonance was presented. The theory behind the operation of MPAs was derived along with equations for calculating the resonance frequency of operation, quality factor and transmitted magnetic field. The operation of MPAs was verified using Ansys Maxwell 2D simulations. A proof of concept demonstration was shown at 1031 Hz along with 2 bps modulation using 28-Element 1D MPA and at 727 Hz with 18 bps BFSK modulation using the 55- Element 2D MPA. It was observed that the efficiency of the 1D pendulum array is about 7 dB higher than the bare coils and 2D array is about 18 dB higher than a coil of same dimensions. Simple circuit models were presented which helps verify the properties of MPA and calculation of Q factor. Direct Antenna Modulation was implemented to achieve higher data rate efficiently in the 2D array prototype. The results presented here demonstrate the feasibility of using high-Q magnetic pendulum arrays for efficiently transmitting Ultra Low Frequencies. We believe a host of other applications beyond underwater communications, such as wireless power transfer and underground localization can benefit from magnetic pendulum arrays. In conclusion we would like to note that magnetic pendulum arrays offer a high-Q solution for storage and transmission of energy at ULF, which may be replacement to conventional coils for various applications in power electronics, filters, antennas and energy harvesting.

APPENDIX A

Derivation of torque between two cylindrical magnets

Assuming a long cylindrical magnet along z axis with radius 'b', magnetized radially along $\hat{x}$

Magnetization: $M\boldsymbol{a}_x$

Magnetic Field outside at a distance r can be written as [27]:

$$B = \mu_0 \frac{Mb^2}{2r^4}[(x^2 - y^2)\boldsymbol{a}_x + 2xy\boldsymbol{a}_y]]$$

Magnetic field inside the magnet can be written as [27]

$$B = \mu_0 \frac{M}{2}\boldsymbol{a}_x$$

Let the angle of rotation of the magnet be θ along z axis

The new magnetization vector can be calculated as

$$\begin{bmatrix} cos\theta & -sin\theta \\ sin\theta & cos\theta \end{bmatrix}\begin{bmatrix} M \\ 0 \end{bmatrix} = Mcos\theta\boldsymbol{a}_x + Msin\theta\boldsymbol{a}_y$$

The field outside now can be written as

$$B = \mu_0 \frac{Mb^2}{2r^4}[(x^2 - y^2)\boldsymbol{a}_x + 2xy\boldsymbol{a}_y]]cos\theta + \mu_0 \frac{Mb^2}{2r^4}[(y^2 - x^2)\boldsymbol{a}_y + 2xy\boldsymbol{a}_x]]sin\theta$$

The field inside now can be written as

$$B = \mu_0 \frac{Mcos\theta}{2}\boldsymbol{a}_x + \mu_0 \frac{Msin\theta}{2}\boldsymbol{a}_y$$

To calculate the torque τ_z between the magnets we can write [28]

$$\tau_z = \iiint (M \times B) dxdydz$$

$$M \times B = \begin{vmatrix} \hat{x} & \hat{y} & \hat{z} \\ Mcos\theta & Msin\theta & 0 \\ B_x & B_y & 0 \end{vmatrix} = Mcos\theta B_y - Msin\theta B_x$$

$$B_x = \mu_0 \frac{Mb^2}{2r^4} [(x^2 - y^2)cos\theta + 2xysin\theta]$$

$$B_y = \mu_0 \frac{Mb^2}{2r^4} [2xycos\theta + (y^2 - x^2)sin\theta]$$

$$Mcos\theta B_y - Msin\theta B_x = Mcos\theta \left[\mu_0 \frac{Mb^2}{2r^4} [2xycos\theta + (y^2 - x^2)sin\theta]\right] - Msin\theta \left[\mu_0 \frac{Mb^2}{2r^4} [(x^2 - y^2)cos\theta + 2xysin\theta]\right]$$

Simplifying

$$= \frac{\mu_o M^2 b^2}{2r^4} \left[(2xycos^2\theta + (y^2 - x^2)cos\theta sin\theta) + \left((y^2 - x^2)sin\theta cos\theta - (2xy)\sin^2\theta\right)\right]$$

$$r = \sqrt{x^2 + y^2}$$

$$= \frac{\mu_o M^2 b^2}{2} \left[2 \frac{(y^2 - x^2)}{(x^2 + y^2)^2} sin\theta cos\theta + 2xy(\cos^2\theta - \sin^2\theta)\right]$$

The second term is odd in y and hence the integration would be zero.

Integrating the first term

$$\tau_z = \frac{\mu_o M^2 b^2}{2} sin2\theta \iiint_{-zyx}^{zyx} \frac{(y^2 - x^2)}{(x^2 + y^2)^2} dxdydz$$

$$z\ limits:\ -\frac{w}{2}\ to\frac{w}{2}\ \ (w\ is\ the\ height\ of\ the\ magnets)$$

$$y\ limits:\ -b\ to\ b\ (b\ is\ the\ radius\ of\ the\ magnets)$$

$$x\ limits: d-\sqrt{b^2-y^2}\ to\ d+\sqrt{b^2+y^2}\ \ (d\ is\ the\ distance\ between\ centers\ of\ magnets)$$

Integration was done in Wolfram Alpha

Integrating wrt *x*

$$\int \frac{(y^2-x^2)}{(x^2+y^2)^2}dx = \frac{x}{x^2+y^2}$$

Applying x limits

$$\frac{d+\sqrt{b^2-y^2}}{\left(d+\sqrt{b^2-y^2}\right)^2+y^2}-\frac{d-\sqrt{b^2-y^2}}{\left(d-\sqrt{b^2-y^2}\right)^2+y^2}$$

Integrating wrt *y*

$$\int \frac{d+\sqrt{b^2-y^2}}{\left(d+\sqrt{b^2-y^2}\right)^2+y^2}-\frac{d-\sqrt{b^2-y^2}}{\left(d-\sqrt{b^2-y^2}\right)^2+y^2}\ dy$$

$$=\frac{(d^2-b^2)\tan^{-1}\left(\frac{y}{\sqrt{b^2-y^2}}\right)+(b^2+d^2)\tan^{-1}\left(\frac{y(b^2+d^2)}{(b^2-d^2)\sqrt{b^2-y^2}}\right)}{2d^2}$$

Applying y limits (since the function is even in y, we do $2\int_0^b f(y)dy$)

$$= 2\,\frac{(d^2 - b^2)\tan^{-1}\left(\frac{b}{\sqrt{b^2 - b^2}}\right) + (b^2 + d^2)\tan^{-1}\left(\frac{b(b^2 + d^2)}{(b^2 - d^2)\sqrt{b^2 - b^2}}\right)}{2d^2}$$

$$= \frac{1}{d^2}\left[(d^2 - b^2)\frac{\pi}{2} + (b^2 + d^2)\frac{-\pi}{2}\right] \quad \text{(since } (b^2 - d^2) is - ve \text{)}$$

$$= \frac{\pi b^2}{d^2}$$

Integrating wrt *z* is just multiplying by w

The final integral turns out to be

$$\tau_z = \frac{\pi \mu_0 M^2 b^4 w sin2\theta}{2d^2}$$

References

[1] Pozar, D. M. Microwave Engineering. (J. Wiley, 2005).

[2] D. Roddy and J. Coolen, Electronic Communications (4th Ed.). Upper Saddle River, NJ, USA: Prentice-Hall, Inc., 1995..

[3] M. Burrows, ELF Communications Antennas. IEE ElectromagneticWaves Series, Peter Peregrinus, 1978..

[4] Chu, L. J. Physical limitations of omni-directional antennas. J. Appl. Phys. 19, 1163-1175 (1948).

[5] Watt, A. D. VLF Radio Engineering. (Pergamon Press, 1967).

[6] Azad, U. & Wang, Y. E. Direct antenna modulation (DAM) for enhanced capacity performance of near-field communication (NFC) link. IEEE Trans. on Circuits Syst. I, Reg. Papers, 61, 902-910 (2014).

[7] de Soria-Santacruz, M., Bautista, G., Gettliffe, G.V., Martinez-Sanchez, M. & Miller, D. W. Design of a space-borne antenna for controlled removal of energetic Van Allen belt protons. IEEE Aerospace Conf. 1- 20 (2014).

[8] Gigliotti, A. *et al.* Generation of polarized shear alfven waves by a rotating magnetic field source. *Phys. Plasmas*. **16,** 092106 (2009).

[9] B. Dolgin, S. Cotten, and J. Zellner. Magnetic antennas for ultra low frequency and very low frequency radiation. Dec. 24 2015. US Patent App. 14/311,558.

[10] Burch, H., Garraud, A., Mitchell, M.F., Moore, R.C. & Arnold, D.P. Experimental generation of ELF radio signals using a rotating magnet. IEEE Trans. Antennas Propag. 66, 11. 6265-6272 (2017).

[11] Selvin, S., Prasad, S., Huang, Y., & Wang, Y.E. Spinning magnet antenna for VLF transmitting. IEEE International Symposium on Antennas and Propagation USNC/URSI National Radio Science Meeting. 1477-1478(2017). 10.1109/APUSNCURSINRSM.2017.8072781.

[12] Madanayake, A. et al. Energy-efficient ULF/VLF transmitters based on mechanically-rotating dipoles. MERCon. 230–235(2017).

[13] Prasad, M. N. S., Selvin, S., Tok, R. U., Huang, Y., & Wang, Y.E. Directly modulated spinning magnet arrays for ULF communications. IEEE Radio and Wireless Symp. 171-173 (2018).

[14] S. P. M. Nagaraja, “Going beyond Chu’s limit: ULF radiation with directly modulated spinning magnet arrays,” M.S. thesis, Dept. Sci. Elect. Eng., Univ. California, Los Angeles, Los Angeles, CA, USA, 2017.

[15] Majid Manteghi. A Navigation and Positining System for Unmanned Underwater Vehicles Based on a Mechanical Antenna. IEEE International Symposium on Antennas and Propagation USNC/URSI National Radio Science Meeting. (2017).

[16] Navid Barani, Kamal Sarabandi, "A Frequency Multiplier and Phase Modulation Approach for Mechanical Antennas Operating at Super Low Frequency (SLF) Band", *Antennas and Propagation and USNC-URSI Radio Science Meeting 2019 IEEE International Symposium on*, pp. 2169-2170, 2019.

[17] Olutosin Charles Fawole, Massood Tabib-Azar. An Electromechanically Modulated Permanent Magnet Antenna for Wireless Communication in Harsh Electromagnetic Environments. IEEE Trans. Antennas Propag. 65, 12. (2017).

[18] Bickford, J. A., McNabb, R. S., Ward, P. A., Freeman, D. K. & Weinberg, M. S. Low frequency mechanical antennas: electrically short transmitters from mechanically-actuated dielectrics. IEEE International Symposium on Antennas and Propagation USNC/URSI National Radio Science Meeting. 1475–1476 (2017). 10.1109/APUSNCURSINRSM.2017.8072780.

[19] Xu, J., Leung, C.M., Zhuang, X., Li, J., Bhardwaj, S., Volakis, J., Viehland, D. A Low Frequency Mechanical Transmitter Based on Magnetoelectric Heterostructures Operated at Their Resonance Frequency. Sensors 2019, 19, 853.

[20] Kemp, Mark. A., et al. A high Q piezoelectric resonator as a portable VLF transmitter. Nat. Commun.10, 1715; https://rdcu.be/bMBfq (2019).

[21] Mysore Nagaraja, S.P., Tok, R.U. & Wang, Y. E. Magnetic pendulum arrays for ULF transmission. IEEE International Symposium on Antennas and Propagation USNC/URSI National Radio Science Meeting.71-72 (2018). 10.1109/APUSNCURSINRSM.2018.8609255.

[22] Azad, U. & Wang, Y. E. Direct antenna modulation scheme for enhanced capacity performance of near-field communication link. IEEE IWAT.88-91(2012)..

[23] Weickhmann, M. Nd-fe-b magnets, properties and applications. Vacuumschmelze GmbH and Co (2009).

[24] X. Xu, H. C. Jing, and Y. E. Wang, “High Speed Pulse Radiation from Switched Electrically Small Antennas,” 2006 IEEE Int. Symp. Antennas Propag., pp. 167–170, 2006.

[25] X. Xu and Y. E. Wang, “Beyond the efficiency bandwidth limit with switched electrically small antennas,” in IEEE Antennas and Propagation Society, AP-S International Symposium (Digest), 2007, pp. 2261–2264..

[26] X. J. Xu and Y. E. Wang, “A Direct Antenna Modulation (DAM) Transmitter with a Switched Electrically Small Antenna,” 2010 Int. Work. Antenna Technol., pp. 2–5, 2010.

[27] K.T. McDonald, “Long Rod with Uniform Magnetization Transverse to its Axis,” Princeton University, Nov. 1999.

[28] Griffiths, D. J. Introduction to Electrodynamics. (Prentice Hall, 1999).